Electronic Supplementary Material (ESI) for Physical Chemistry Chemical Physics.
This journal is © the Owner Societies 2021

Supplementary Information for "Determining chemical exchange rate constants in nanoemulsions using nuclear magnetic resonance."

Zhaoyuan Gong

Department of Chemistry, University of Miami, Coral Gables, Florida 33146, USA

Mohammad Hossein Tootoonchi

Diabetes Research Institute, University of Miami

Miller School of Medicine, Miami, FL 33136, USA

Christopher A. Fraker*

Diabetes Research Institute, University of Miami

Miller School of Medicine, Miami, FL 33136,USA

Jamie D. Walls†

Department of Chemistry, University of Miami, Coral Gables, Florida 33146,USA

(Dated: August 3, 2021)

Abstract

Supplementary information on the basic applications of Bloch-McConnell theory used to describe the NMR dilutions experiments in this work. Additional information on fitting spectral and kinetic parameters is also provided.

CONTENTS

I. BLOCH-MCCONNELL SIMULATIONS OF ISOFLURANE IN AN FC43 EMULSION

The Bloch-McConnell equations can be solved for the isolated F_3H^α and F_2H^β spin subgroups in isoflurane, respectively [See Fig. S8 or Fig. 2**a** of main text]. For the F_3H^α group, the relevant spin evolution involves the exchange between the spin subspaces $\left\{\widehat{I}^\alpha_{+,\mathrm{aq}}, \widehat{S}^\alpha_Z\widehat{I}^\alpha_{+,\mathrm{aq}}, \left(\widehat{S}^\alpha_{Z1}\widehat{S}^\alpha_{Z2}+\widehat{S}^\alpha_{Z1}\widehat{S}^\alpha_{Z3}+\widehat{S}^\alpha_{Z2}\widehat{S}^\alpha_{Z3}\right)\widehat{I}^\alpha_{+,\mathrm{aq}}, \widehat{S}^\alpha_{Z1}\widehat{S}^\alpha_{Z2}\widehat{S}^\alpha_{Z3}\widehat{I}^\alpha_{+,aq}\right\}$ and $\left\{\widehat{I}^\alpha_{+,\mathrm{Emul}}, \widehat{S}^\alpha_Z\widehat{I}^\alpha_{+,\mathrm{Emul}}, \left(\widehat{S}^\alpha_{Z1}\widehat{S}^\alpha_{Z2}+\widehat{S}^\alpha_{Z1}\widehat{S}^\alpha_{Z3}+\widehat{S}^\alpha_{Z2}\widehat{S}^\alpha_{Z3}\right)\widehat{I}^\alpha_{+,\mathrm{Emul}}, \widehat{S}^\alpha_{Z1}\widehat{S}^\alpha_{Z2}\widehat{S}^\alpha_{Z3}\widehat{I}^\alpha_{+,\mathrm{Emul}}\right\}$, where $\widehat{S}^\alpha_Z = \sum_{j=1}^{3}\widehat{S}^\alpha_{Zj}$ represents the total $\hat{z}$-magnetization for the ^{19}F nuclei in the CF_3 group, and $\widehat{I}^\alpha_+$ denotes the single-quantum spin coherence operator for the H^α spin [See Fig. S8]. In this case, the Bloch-McConnell equations for the F_3H^α spin subsystem are given by:

$$\frac{d}{dt}\begin{pmatrix} \left\langle \widehat{I}^\alpha_{+,\mathrm{aq}}\right\rangle(t) \\ \left\langle \widehat{S}^\alpha_Z\widehat{I}^\alpha_{+,\mathrm{aq}}\right\rangle(t) \\ \left\langle \left(\widehat{S}^\alpha_{Z1}\widehat{S}^\alpha_{Z2}+\widehat{S}^\alpha_{Z1}\widehat{S}^\alpha_{Z3}+\widehat{S}^\alpha_{Z2}\widehat{S}^\alpha_{Z3}\right)\widehat{I}^\alpha_{+,\mathrm{aq}}\right\rangle(t) \\ \left\langle \widehat{S}^\alpha_{Z1}\widehat{S}^\alpha_{Z2}\widehat{S}^\alpha_{Z3}\widehat{I}^\alpha_{+,\mathrm{aq}}\right\rangle(t) \\ \left\langle \widehat{I}^\alpha_{+,\mathrm{Emul}}\right\rangle(t) \\ \left\langle \widehat{S}^\alpha_Z\widehat{I}^\alpha_{+,\mathrm{Emul}}\right\rangle(t) \\ \left\langle \left(\widehat{S}^\alpha_{Z1}\widehat{S}^\alpha_{Z2}+\widehat{S}^\alpha_{Z1}\widehat{S}^\alpha_{Z3}+\widehat{S}^\alpha_{Z2}\widehat{S}^\alpha_{Z3}\right)\widehat{I}^\alpha_{+,\mathrm{Emul}}\right\rangle(t) \\ \left\langle \widehat{S}^\alpha_{Z1}\widehat{S}^\alpha_{Z2}\widehat{S}^\alpha_{Z3}\widehat{I}^\alpha_{+,\mathrm{Emul}}\right\rangle(t) \end{pmatrix} = \begin{pmatrix} \widehat{\widehat{\mathcal{L}}}^\alpha_{\mathrm{aq,aq}} & \widehat{\widehat{\mathcal{L}}}^\alpha_{\mathrm{aq,Emul}} \\ \widehat{\widehat{\mathcal{L}}}^\alpha_{\mathrm{Emul,aq}} & \widehat{\widehat{\mathcal{L}}}^\alpha_{\mathrm{Emul,Emul}} \end{pmatrix} \begin{pmatrix} \left\langle \widehat{I}^\alpha_{+,\mathrm{aq}}\right\rangle(t) \\ \left\langle \widehat{S}^\alpha_Z\widehat{I}^\alpha_{+,\mathrm{aq}}\right\rangle(t) \\ \left\langle \left(\widehat{S}^\alpha_{Z1}\widehat{S}^\alpha_{Z2}+\widehat{S}^\alpha_{Z1}\widehat{S}^\alpha_{Z3}+\widehat{S}^\alpha_{Z2}\widehat{S}^\alpha_{Z3}\right)\widehat{I}^\alpha_{+,\mathrm{aq}}\right\rangle(t) \\ \left\langle \widehat{S}^\alpha_{Z1}\widehat{S}^\alpha_{Z2}\widehat{S}^\alpha_{Z3}\widehat{I}^\alpha_{+,\mathrm{aq}}\right\rangle(t) \\ \left\langle \widehat{I}^\alpha_{+,\mathrm{Emul}}\right\rangle(t) \\ \left\langle \widehat{S}^\alpha_Z\widehat{I}^\alpha_{+,\mathrm{Emul}}\right\rangle(t) \\ \left\langle \left(\widehat{S}^\alpha_{Z1}\widehat{S}^\alpha_{Z2}+\widehat{S}^\alpha_{Z1}\widehat{S}^\alpha_{Z3}+\widehat{S}^\alpha_{Z2}\widehat{S}^\alpha_{Z3}\right)\widehat{I}^\alpha_{+,\mathrm{Emul}}\right\rangle(t) \\ \left\langle \widehat{S}^\alpha_{Z1}\widehat{S}^\alpha_{Z2}\widehat{S}^\alpha_{Z3}\widehat{I}^\alpha_{+,\mathrm{Emul}}\right\rangle(t) \end{pmatrix} \tag{S1}$$

where $\widehat{\widehat{\mathcal{L}}}^\alpha_{\mathrm{aq,aq}}$, $\widehat{\widehat{\mathcal{L}}}^\alpha_{\mathrm{aq,Emul}}$, $\widehat{\widehat{\mathcal{L}}}^\alpha_{\mathrm{Emul,aq}}$, and $\widehat{\widehat{\mathcal{L}}}^\alpha_{\mathrm{Emul,Emul}}$ are 4×4 matrices given by:

$$\widehat{\widehat{\mathcal{L}}}^\alpha_{\mathrm{aq,aq}} = \begin{pmatrix} -i\omega^\alpha_{\mathrm{aq}} - \frac{1}{T^{*,\alpha}_{2,\mathrm{aq}}} - k_F[\mathrm{Emul}] & -i2\pi J^\alpha_{HF,\mathrm{aq}} & 0 & 0 \\ -i\frac{3}{2}\pi J^\alpha_{HF,\mathrm{aq}} & -i\omega^\alpha_{\mathrm{aq}} - \frac{1}{T^{*,\alpha}_{2,\mathrm{aq}}} - k_F[\mathrm{Emul}] & -i\pi J^\alpha_{HF,\mathrm{aq}} & 0 \\ 0 & -i\pi J^\alpha_{HF,\mathrm{aq}} & -i\omega^\alpha_{\mathrm{aq}} - \frac{1}{T^{*,\alpha}_{2,\mathrm{aq}}} - k_F[\mathrm{Emul}] & -i6\pi J^\alpha_{HF,\mathrm{aq}} \\ 0 & 0 & -i\frac{\pi}{2}J^\alpha_{HF,\mathrm{aq}} & -i\omega^\alpha_{aq} - \frac{1}{T^{*,\alpha}_{2,\mathrm{aq}}} - k_F[\mathrm{Emul}] \end{pmatrix} \tag{S2}$$

$$\widehat{\widehat{\mathcal{L}}}^\alpha_{\mathrm{Emul,Emul}} = \begin{pmatrix} -i\omega^{\alpha\left(\phi^{\mathrm{Org}}_{\mathrm{Iso}}\right)}_{\mathrm{Emul}} - \frac{1}{T^{*,\alpha}_{2,\mathrm{Emul}}} - k_B & -i2\pi J^\alpha_{HF,\mathrm{Emul}} & 0 & 0 \\ -i\frac{3}{2}\pi J^\alpha_{HF,\mathrm{Emul}} & -i\omega^{\alpha\left(\phi^{\mathrm{Org}}_{\mathrm{Iso}}\right)}_{\mathrm{Emul}} - \frac{1}{T^{*,\alpha}_{2,\mathrm{Emul}}} - k_B & -i\pi J^\alpha_{HF,\mathrm{Emul}} & 0 \\ 0 & -i\pi J^\alpha_{HF,\mathrm{Emul}} & -i\omega^{\alpha\left(\phi^{\mathrm{Org}}_{\mathrm{Iso}}\right)}_{\mathrm{Emul}} - \frac{1}{T^{*,\alpha}_{2,\mathrm{Emul}}} - k_B & -i6\pi J^\alpha_{HF,\mathrm{Emul}} \\ 0 & 0 & -i\frac{\pi}{2}J^\alpha_{HF,\mathrm{Emul}} & -i\omega^{\alpha\left(\phi^{\mathrm{Org}}_{\mathrm{Iso}}\right)}_{\mathrm{Emul}} - \frac{1}{T^{*,\alpha}_{2,\mathrm{Emul}}} - k_B \end{pmatrix} \tag{S3}$$

$$\widehat{\widehat{\mathcal{L}}}^\alpha_{\mathrm{aq,Emul}} = \begin{pmatrix} k_B & 0 & 0 & 0 \\ 0 & k_B & 0 & 0 \\ 0 & 0 & k_B & 0 \\ 0 & 0 & 0 & k_B \end{pmatrix} \tag{S4}$$

$$\widehat{\widehat{\mathcal{L}}}^\alpha_{\mathrm{Emul,aq}} = \begin{pmatrix} k_F[\mathrm{Emul}] & 0 & 0 & 0 \\ 0 & k_F[\mathrm{Emul}] & 0 & 0 \\ 0 & 0 & k_F[\mathrm{Emul}] & 0 \\ 0 & 0 & 0 & k_F[\mathrm{Emul}] \end{pmatrix} \tag{S5}$$

where $\omega^{\alpha}_{\text{Emul}}\left(\phi^{\text{Org}}_{\text{Iso}}\right)$ is the effective frequency for the H^{α} resonance in the emulsion droplet, which can be calculated by:

$$\omega^{\alpha}_{\text{Emul}}\left(\phi^{\text{Org}}_{\text{Iso}}\right) = \omega^{\alpha}_{\text{FC43/Iso}}\left(\phi^{\text{Org}}_{\text{Iso}}\right) + \omega^{\text{Emul}}_{\text{offset}} \tag{S6}$$

where $\omega^{\text{Emul}}_{\text{offset}}$ is an empirically determined offset applied to both H^{α} and H^{β} resonances, and $\omega^{\alpha}_{FC43/Iso}\left(\phi^{\text{Org}}_{\text{Iso}}\right) = \gamma|\vec{B}_0|\delta^{\alpha}_{\text{FC43/Iso}}\left(\phi^{\text{Org}}_{\text{Iso}}\right)$, where $\delta^{\alpha}_{\text{FC43/Iso}}\left(\phi^{\text{Org}}_{\text{Iso}}\right)$ is given in Eq. (16) and Fig. **2a** in the main text. In Eq. (S6), $\omega^{\alpha}_{\text{Emul}}\left(\phi^{\text{Org}}_{\text{Iso}}\right)$ is modeled to depend upon the isoflurane composition in the emulsion droplet, $\phi^{\text{Org}}_{\text{Iso}}$ in Eq. (19) of the main text, and hence to depend upon k_F, k_B, and [Emul]:

Additionally, it was assumed in Eq. (S1) that the multi-spin, single-quantum coherences, $\widehat{S}^{\alpha}_{Z}\widehat{I}^{\alpha}_{+}$, $\widehat{S}^{\alpha}_{Z1}\widehat{S}^{\alpha}_{Z2}\widehat{I}^{\alpha}_{+}$, $\widehat{S}^{\alpha}_{Z1}\widehat{S}^{\alpha}_{Z2}\widehat{S}^{\alpha}_{Z3}\widehat{I}^{\alpha}_{+}$, etc., all have the same nominal $T^{*,\alpha}_{2}$ as $\widehat{I}^{\alpha}_{+}$. In this case, Eq. (S1) is solved with the initial boundary conditions at $t = 0$ after application of a $\frac{\pi}{2}$-pulse, where the only nonzero elements at $t = 0$ were $\langle I^{\alpha}_{+,aq}\rangle(0) = \frac{k_B}{k_{\text{exch}}}$ and $\langle I^{\alpha}_{+,\text{Emul}}\rangle(0) = \frac{k_F[\text{Emul}]}{k_{\text{exch}}}$.

Similarly, for the F_2H^{β} spin subsystem, the spin evolution involves the exchange between the spin subspaces $\left\{\widehat{I}^{\beta}_{+,\text{aq}}, \widehat{S}^{\beta}_{Z1}\widehat{I}^{\beta}_{+,\text{aq}}, \widehat{S}^{\beta}_{Z2}\widehat{I}^{\beta}_{+,\text{aq}}, \widehat{S}^{\beta}_{Z1}\widehat{S}^{\beta}_{Z2}\widehat{I}^{\beta}_{+,\text{aq}}\right\}$ and $\left\{\widehat{I}^{\beta}_{+,\text{Emul}}, \widehat{S}^{\beta}_{Z1}\widehat{I}^{\beta}_{+,\text{Emul}}, \widehat{S}^{\beta}_{Z2}\widehat{I}^{\beta}_{+,\text{Emul}}, \widehat{S}^{\beta}_{Z1}\widehat{S}^{\beta}_{Z2}\widehat{I}^{\beta}_{+,\text{Emul}}\right\}$. Note that the two ^{19}F nuclei are chemically inequivalent [See Fig. S8] and can therefore have different scalar spin couplings to the H^{β} spin. In the organic phase, there is a nonzero chemical shift difference between the ^{19}F spins, $\Delta\delta^{\beta,\beta}_{F1F2,\text{Emul}} = 1.19$ ppm, along with a small difference in $^{1}H^{19}F$ spin-spin couplings [$J^{\beta}_{HF1,\text{Emul}} = 70.3$ Hz and $J^{\beta}_{HF2,\text{Emul}} = 72.3$ Hz], whereas in the aqueous phase, $\Delta\delta^{\beta,\beta}_{F1F2,\text{aq}} = 0$ and $J^{\beta}_{HF1,\text{aq}} = J^{\beta}_{HF2,\text{aq}} = J^{\beta}_{HF,\text{aq}} = 71.1$ Hz [see Table 1 of the main text].

The Bloch-McConnell equations in the F_2H^{β} spin subspace are given by:

$$\frac{d}{dt}\begin{pmatrix} \left\langle \widehat{I}^{\beta}_{+,\text{aq}}\right\rangle(t) \\ \left\langle \widehat{S}^{\beta}_{Z1}\widehat{I}^{\beta}_{+,\text{aq}}\right\rangle(t) \\ \left\langle \widehat{S}^{\beta}_{Z2}\widehat{I}^{\beta}_{+,\text{aq}}\right\rangle(t) \\ \left\langle \widehat{S}^{\beta}_{Z1}\widehat{S}^{\beta}_{Z2}\widehat{I}^{\beta}_{+,\text{aq}}\right\rangle(t) \\ \left\langle \widehat{I}^{\beta}_{+,\text{Emul}}\right\rangle(t) \\ \left\langle \widehat{S}^{\beta}_{Z1}\widehat{I}^{\beta}_{+,\text{Emul}}\right\rangle(t) \\ \left\langle \widehat{S}^{\beta}_{Z2}\widehat{I}^{\beta}_{+,\text{Emul}}\right\rangle(t) \\ \left\langle \widehat{S}^{\beta}_{Z1}\widehat{S}_{Z2,\alpha}\widehat{I}^{\beta}_{+,\text{Emul}}\right\rangle(t) \end{pmatrix} = \begin{pmatrix} \widehat{\widehat{\mathcal{L}}}^{\beta}_{\text{aq,aq}} & \widehat{\widehat{\mathcal{L}}}^{\beta}_{\text{aq,Emul}} \\ \widehat{\widehat{\mathcal{L}}}^{\beta}_{\text{Emul,aq}} & \widehat{\widehat{\mathcal{L}}}^{\beta}_{\text{Emul,Emul}} \end{pmatrix} \begin{pmatrix} \left\langle \widehat{I}^{\beta}_{+,\text{aq}}\right\rangle(t) \\ \left\langle \widehat{S}^{\beta}_{Z1}\widehat{I}^{\beta}_{+,aq}\right\rangle(t) \\ \left\langle \widehat{S}^{\beta}_{Z2}\widehat{I}^{\beta}_{+,\text{aq}}\right\rangle(t)\rangle \\ \left\langle \widehat{S}^{\beta}_{Z1}\widehat{S}^{\beta}_{Z2}\widehat{I}^{\beta}_{+,\text{aq}}\right\rangle(t)\rangle \\ \left\langle \widehat{I}^{\beta}_{+,\text{Emul}}\right\rangle(t) \\ \left\langle \widehat{S}^{\beta}_{Z1}\widehat{I}^{\beta}_{+,\text{Emul}}\right\rangle(t) \\ \left\langle \widehat{S}^{\beta}_{Z2}\widehat{I}^{\beta}_{+,\text{Emul}}\right\rangle(t) \\ \left\langle \widehat{S}^{\beta}_{Z1}\widehat{S}^{\beta}_{Z2}\widehat{I}^{\beta}_{+,\text{Emul}}\right\rangle(t) \end{pmatrix} \tag{S7}$$

where $\widehat{\widehat{\mathcal{L}}}^{\beta}_{\text{aq,aq}}$, $\widehat{\widehat{\mathcal{L}}}^{\beta}_{\text{aq,Emul}}$, $\widehat{\widehat{\mathcal{L}}}^{\beta}_{\text{Emul,aq}}$, and $\widehat{\widehat{\mathcal{L}}}^{\beta}_{\text{Emul,Emul}}$ are 4×4 matrices given by:

$$\widehat{\widehat{\mathcal{L}}}^{\beta}_{\text{aq,aq}} = \begin{pmatrix} -i\omega^{\beta}_{\text{aq}} - \frac{1}{T^{*,\beta}_{2,\text{aq}}} - k_F[\text{Emul}] & -i2\pi J^{\beta}_{HF,\text{aq}} & -i2\pi J^{\beta}_{HF,\text{aq}} & 0 \\ -i\frac{\pi}{2}J^{\beta}_{HF,\text{aq}} & -i\omega^{\beta}_{\text{aq}} - \frac{1}{T^{*,\beta}_{2,\text{aq}}} - k_F[\text{Emul}] & 0 & -i2\pi J^{\beta}_{HF,\text{aq}} \\ -i\frac{\pi}{2}J^{\beta}_{HF,\text{aq}} & 0 & -i\omega^{\beta}_{\text{aq}} - \frac{1}{T^{*,\beta}_{2,\text{aq}}} - k_F[\text{Emul}] & -2i\pi J^{\beta}_{HF,\text{aq}} \\ 0 & -i\frac{\pi}{2}J^{\beta}_{HF,\text{aq}} & -i\frac{\pi}{2}J^{\beta}_{HF,\text{aq}} & -i\omega^{\beta}_{\text{aq}} - \frac{1}{T^{*,\beta}_{2,\text{aq}}} - k_F[\text{Emul}] \end{pmatrix} \tag{S8}$$

$$\widehat{\widehat{\mathcal{L}}}^{\beta}_{\text{Emul,Emul}} = \begin{pmatrix} -i\omega^{\beta\left(\phi^{\text{Org}}_{\text{Iso}}\right)}_{\text{Emul}} - \frac{1}{T^{*,\beta}_{2,\text{Emul}}} - k_B & -i2\pi J^{\beta}_{HF1,\text{Emul}} & -i2\pi J^{\beta}_{HF2,\text{Emul}} & 0 \\ -i\frac{\pi}{2} J^{\beta}_{HF1,\text{Emul}} & -i\omega^{\beta\left(\phi^{\text{Org}}_{\text{Iso}}\right)}_{\text{Emul}} - \frac{1}{T^{*,\beta}_{2,\text{Emul}}} - k_B & 0 & -i2\pi J^{\beta}_{HF2,\text{Emul}} \\ -i\frac{\pi}{2} J^{\beta}_{HF2,\text{Emul}} & 0 & -i\omega^{\beta\left(\phi^{\text{Org}}_{\text{Iso}}\right)}_{\text{Emul}} - \frac{1}{T^{*,\beta}_{2,\text{Emul}}} - k_B & -2i\pi J^{\beta}_{HF1,\text{Emul}} \\ 0 & -i\frac{\pi}{2} J^{\beta}_{HF2,\text{Emul}} & -i\frac{\pi}{2} J^{\beta}_{HF1,\text{Emul}} & -i\omega^{\beta\left(\phi^{\text{Org}}_{\text{Iso}}\right)}_{\text{Emul}} - \frac{1}{T^{*,\beta}_{2,\text{Emul}}} - k_B \end{pmatrix} \tag{S9}$$

$$\widehat{\widehat{\mathcal{L}}}^{\beta}_{\text{aq,Emul}} = \begin{pmatrix} k_B & 0 & 0 & 0 \\ 0 & k_B & 0 & 0 \\ 0 & 0 & k_B & 0 \\ 0 & 0 & 0 & k_B \end{pmatrix} \tag{S10}$$

$$\widehat{\widehat{\mathcal{L}}}^{\beta}_{\text{Emul,aq}} = \begin{pmatrix} k_F[\text{Emul}] & 0 & 0 & 0 \\ 0 & k_F[\text{Emul}] & 0 & 0 \\ 0 & 0 & k_F[\text{Emul}] & 0 \\ 0 & 0 & 0 & k_F[\text{Emul}] \end{pmatrix} \tag{S10}$$

where

$$\omega^{\beta}_{\text{Emul}}\left(\phi^{\text{Org}}_{\text{Iso}}\right) = \omega^{\beta}_{\text{FC43/Iso}}\left(\phi^{\text{Org}}_{\text{Iso}}\right) + \omega^{\text{Emul}}_{\text{offset}} \tag{S11}$$

with $\omega^{\beta}_{\text{FC43/Iso}}\left(\phi^{\text{Org}}_{\text{Iso}}\right) = \gamma|\vec{B}_0|\delta^{\beta}_{\text{FC43/Iso}}\left(\phi^{\text{Org}}_{\text{Iso}}\right)$, where $\delta^{\beta}_{\text{FC43/Iso}}\left(\phi^{\text{Org}}_{\text{Iso}}\right)$ is given in Eq. (17) and Fig. 2**a** in the main text.

In writing Eq. (S7), the effects of the ^{19}F-^{19}F scalar spin-spin coupling have been neglected since at a field strength of 300 MHz, the fluorine chemical shift difference was $\left|\Delta\nu^{\beta,\beta}_{F1F2}\right| =$ 335.54 Hz, which was around a factor of two larger than $J^{\beta,\beta}_{F1F2} = 164.2$ Hz. With this simplifying assumption, Eq. (S1) was solved with the initial boundary conditions at $t = 0$ after application of a $\frac{\pi}{2}$-pulse with the only nonzero elements given by $\langle\widehat{I}^{\beta}_{+,\text{aq}}\rangle(0) = \frac{k_B}{k_{\text{exch}}}$ and $\langle\widehat{I}^{\beta}_{+,\text{Emul}}\rangle(0) = \frac{k_F[\text{Emul}]}{k_{\text{exch}}}$. With the above results, the contributions of the F_2H^{β} group to the FID is simply given by FID$^{\beta}$(t)= $\langle\widehat{I}^{\beta}_{+,\text{aq}}\rangle(t) + \langle\widehat{I}^{\beta}_{+,\text{Emul}}\rangle(t)$.

The overall FID from a $\frac{\pi}{2}$-pulse experiment can be calculated by:

$$\text{FID}(t) = \chi_{\alpha\beta}\text{FID}^{\alpha}(t) + \text{FID}^{\beta}(t) \tag{S12}$$

where $\chi_{\alpha\beta} = \frac{\text{Integral of H}^{\alpha}\text{ signal}}{\text{Integral of H}^{\beta}\text{ signal}} \leq 1$. While $\chi_{\alpha\beta} = 1$ for isoflurane in a pure saline solution since there is only one H^{α} spin and one H^{β} spin per isoflurane molecule, it was found that $\chi_{\alpha\beta} < 1$ for all dilutions due to differences in the effects of the water presaturation pulse on the H^{α} and H^{β} resonances as shown in Fig. 6**b** of the main text.

TABLE I. Dilution protocol of the emulsion (spectra were given in Fig. 3 of main text).

Dilution #	V_{Emul} (ul)	$V_{\text{D2O/Iso/Saline}}$ (ul)	[Emul] (nM)	$[\text{Iso}]_{\text{tot}}$ (mM)
0 (undiluted)	500	0	172.77	659.60
1	600	100	148.09	567.69
2	250	250	86.39	337.90
3	80	420	27.64	119.14
4	50	450	17.28	80.54
5	30	470	10.37	54.80
6	20	480	6.91	41.94
7	10	490	3.46	29.07
8	8	500	2.72	26.33
9	5	500	1.71	22.57
10	3	500	1.03	20.04
11	2	500	0.693	18.76
D2O/Isoflurane/Saline	0	500	0	16.20

A. Determining $\delta^{\alpha/\beta}_{\mathbf{obs}}$ and $\Delta\nu^{\alpha/\beta}_{\frac{1}{2},\mathbf{obs}}$ in isoflurane dilution spectra

From the experimental dilution spectra (where samples were prepared using the dilution protocol in Table I), $\delta^{\alpha/\beta}_{\text{obs}}$ and $\Delta\nu^{\alpha/\beta}_{\frac{1}{2},\text{obs}}$ were determined and used as inputs into Eq. (15) in the main text in order to calculate k_F and k_B. However, the fine structure of the H^{α} resonance was only visible in a couple of spectra in addition to overlapping with part of the H^{β} multiplet for a few dilutions [Fig. 3, main text]. To extract the line widths and chemical shifts in such cases, the following procedure was used: for each dilution spectrum, the Bloch equations for both a single IS_3 spin system (representing the H^{α} resonance) and a single IS_1S_2 spin system (representing the H^{β} resonance) were simulated where the spectral parameters (δ^{α}, J^{α}_{HF}, and $T^{*,\alpha}_2$ for the IS_3 subsystem and δ^{β}, $J^{\beta}_{HF,1}$, $J^{\beta}_{HF,2}$, and $T^{*,\beta}_2$ for the IS_1S_2 subsystems) and $\chi_{\alpha\beta}$ were varied in order to minimize the absolute difference between the experimental and simulated spectrum. An example of this procedure applied to a series of dilution spectra is shown in Fig. S1, where the blue spectra are the experimental dilution spectra (same as used in Fig. 3 in the main text), the red spectra are the theoretical spectra calculated using the

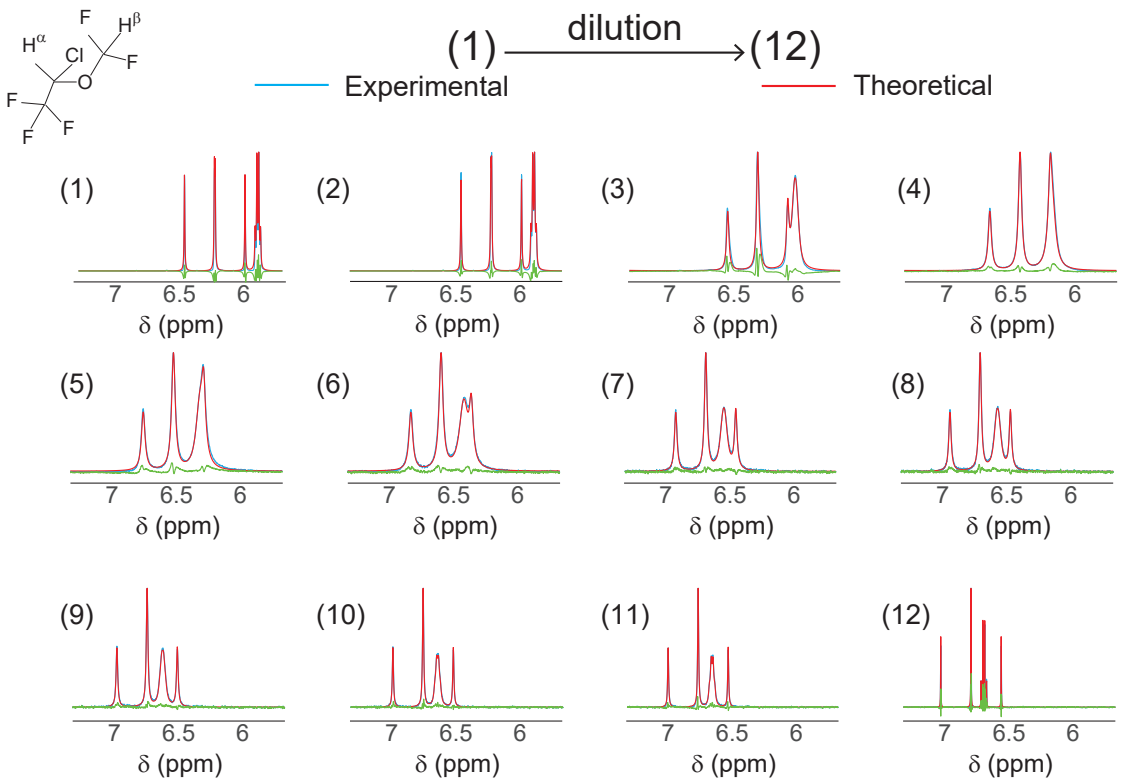

FIG. S1. (blue) Experimental spectra (same as given in Fig. 3 in the main text) and the corresponding (red) simulated spectra assuming a quartet for the H^{α} resonance and a doublet of doublets for the H^{β} resonance. For each spectrum, $\delta_{\text{obs}}^{\alpha/\beta}$, $T_2^{*,\alpha/\beta}$, J_{HF}^{α}, $J_{HF,1}^{\beta}$ and $J_{HF,2}^{\beta}$ were varied to minimize the absolute difference between the simulated and experimental spectra (the green spectra represent the difference between simulation and experiment). From the simulations, $\Delta\nu_{\frac{1}{2},\text{obs}}^{\alpha/\beta}$ and $\delta_{\text{obs}}^{\alpha/\beta}$ were estimated from which k_F and k_B could be determined from Eq. (15) in the main manuscript.

above procedure, and the green spectra represent the difference between the experimental and theoretical spectra. this reduced, simplified, fitting procedure. Denoting the spectral parameters that minimized the total absolute error between experimental and theoretical spectra by $\delta_{\text{optimal}}^{\alpha/\beta}$ and $T_{2,\text{optimal}}^{*,\alpha/\beta}$, the observed chemical shifts and line widths were estimated by $\delta_{\text{obs}}^{\alpha/\beta} = \delta_{\text{optimal}}^{\alpha/\beta}$, which is given in Fig. 2**a** in the main text, and $\Delta\nu_{\frac{1}{2},\text{obs}}^{\alpha/\beta} \approx \frac{1}{\pi T_{2,\text{optimal}}^{*,\alpha/\beta}}$, which is given in Fig. S2. Both $\delta_{\text{obs}}^{\alpha/\beta}$ and $\Delta\nu_{\frac{1}{2},\text{obs}}^{\alpha/\beta}$ were then used as input into Eq. (15) in the main text to determine k_F and k_B, the values of which are given in Table II and Fig. 4 of the main text.

Using these k_F and k_B values, the predicted dilution spectra in the presence of exchange

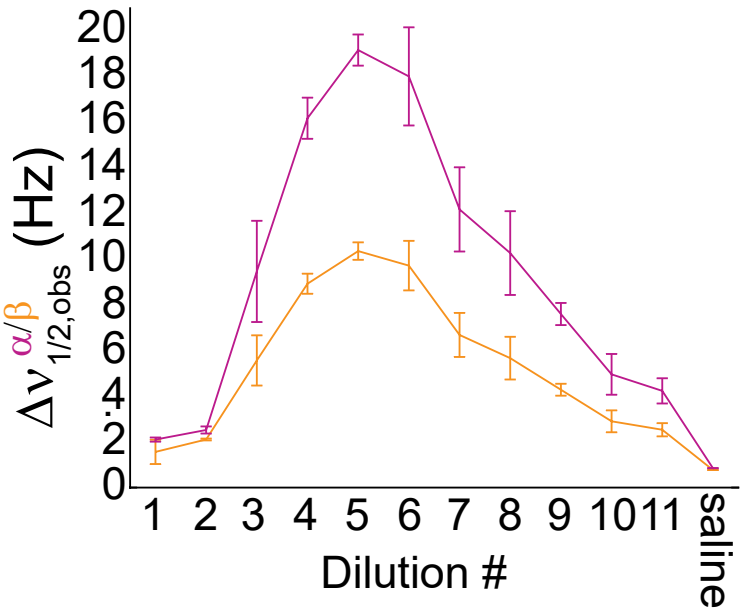

FIG. S2. The line widths for the (magenta) H^{α} and (orange) H^{β} resonances determined from the procedure described in Sec. I A. The error bars represent ± a standard deviation after averaging over three replicates.

were calculated using Bloch-McConnell equations described in Sec. I, an example of which was shown in Fig. 3 of the main manuscript. From these simulations, the differences between the predicted chemical shifts, $\Delta\delta_{\mathrm{Error}}^{\alpha/\beta} = \delta_{\mathrm{obs}}^{\alpha/\beta} - \delta_{\mathrm{predicted}}^{\alpha/\beta}$, and line widths, $\Delta\Delta\nu_{\frac{1}{2},\mathrm{Error}}^{\alpha/\beta} = \Delta\nu_{\frac{1}{2},\mathrm{obs}}^{\alpha/\beta} - \Delta\nu_{\frac{1}{2},\mathrm{predicted}}^{\alpha/\beta}$ are shown in Fig. S3**a** and Fig. S3**b**, respectively. In this case, the absolute differences in chemical shifts from the exchange model presented in the paper and the observed chemical shifts were $\left\langle \left| \Delta\sigma_{\mathrm{Error}}^{\beta} \right| \right\rangle = (2.3 \pm 1.5) \times 10^{-3}$ ppm and $\langle |\Delta\sigma_{\mathrm{Error}}^{\alpha}| \rangle = (2.8 \pm 2.4) \times 10^{-3}$ ppm, while the absolute differences in line widths from the exchange model and the observed line widths were $\left\langle \left| \Delta\Delta\nu_{\frac{1}{2},\mathrm{Error}}^{\beta} \right| \right\rangle = (0.18 \pm 0.12)$ Hz and $\left\langle \left| \Delta\Delta\nu_{\frac{1}{2},\mathrm{Error}}^{\alpha} \right| \right\rangle = (0.39 \pm 0.29)$ Hz.

B. Tolerances of k_F and k_B to variations in chemical shifts and transverse relaxation times

As discussed in the main text, it is possible that $\delta_{\mathrm{aq}}^{\alpha/\beta}$, $\delta_{\mathrm{Emul}}^{\alpha/\beta}$, $T_{2,\mathrm{aq}}^{*,\alpha/\beta}$, and $T_{2,\mathrm{Emul}}^{*,\alpha/\beta}$ could deviate from the values given in Table 1. We will now estimate the resulting errors in k_F

TABLE II. The NMR-determined k_F and k_B parameters given in Fig. 4 of the main text.

Dilution	[Emul] (nM)	k_F ($\times 10^{11}\mathrm{M}^{-1}\mathrm{s}^{-1}$)	k_B ($\times 10^{3}\mathrm{s}^{-1}$)
dilution 2	86.39	4.86 ± 1.31	1.85 ± 0.59
dilution 3	27.64	5.36 ± 1.22	4.24 ± 1.14
dilution 4	17.28	4.95 ± 0.34	5.76 ± 0.42
dilution 5	10.37	5.04 ± 0.37	7.59 ± 0.58
dilution 6	6.91	4.46 ± 0.32	8.79 ± 1.03
dilution 7	3.46	4.37 ± 0.60	10.10 ± 0.96
dilution 8	2.72	4.42 ± 0.54	10.50 ± 1.11
dilution 9	1.71	4.38 ± 0.92	10.40 ± 0.82
dilution 10	1.03	4.86 ± 0.67	11.70 ± 1.66
dilution 11	0.69	4.13 ± 0.77	9.88 ± 1.00

and k_B to such deviations. Since:

$$\begin{aligned}
\frac{\partial \mathrm{Prob}_{\mathrm{Emul,eq}}}{\partial \omega_{\mathrm{aq}}^{\alpha/\beta}} &= -\frac{1}{\Delta\omega^{\alpha/\beta}} + \frac{\omega_{\mathrm{obs}} - \omega_{\mathrm{aq}}^{\alpha/\beta}}{\left(\Delta\omega^{\alpha/\beta}\right)^2} = \frac{\omega_{\mathrm{obs}}^{\alpha/\beta} - \omega_{\mathrm{Emul}}^{\alpha/\beta}}{\left(\Delta\omega^{\alpha/\beta}\right)^2} \\
&= \frac{\mathrm{Prob}_{\mathrm{Emul,eq}} - 1}{\Delta\omega^{\alpha/\beta}} \\
\frac{\partial \mathrm{Prob}_{\mathrm{Emul,eq}}}{\partial \omega_{\mathrm{Emul}}^{\alpha/\beta}} &= -\frac{\omega_{\mathrm{obs}} - \omega_{\mathrm{aq}}}{\left(\Delta\omega^{\alpha/\beta}\right)^2} = -\frac{\mathrm{Prob}_{\mathrm{Emul,eq}}}{\Delta\omega^{\alpha/\beta}}
\end{aligned} \tag{S13}$$

we have from Eq. (15) in the main text:

$$\begin{aligned}
\frac{\partial k_F}{\partial \omega_{\mathrm{aq}}^{\alpha/\beta}} &= \frac{\partial \left(\frac{\left(\Delta\omega^{\alpha/\beta}\right)^2 \mathrm{Prob}_{\mathrm{Emul,eq}}^2 (1 - \mathrm{Prob}_{\mathrm{Emul,eq}})}{[\mathrm{Emul}]\left(\pi\Delta\nu_{\frac{1}{2},\mathrm{obs}}^{\alpha/\beta} - \left\langle \frac{1}{T_2^{*,\alpha/\beta}} \right\rangle\right)} \right)}{\partial \omega_{\mathrm{aq}}^{\alpha/\beta}} \\
&= \frac{k_F}{\Delta\omega^{\alpha/\beta}} \left(1 - \frac{2}{\mathrm{Prob}_{\mathrm{Emul,eq}}} + (1 - \mathrm{Prob}_{\mathrm{Emul,eq}}) \frac{T_{2,\mathrm{exch}}}{T_{2\Delta}} \right) \\
\frac{\partial k_B}{\partial \omega_{\mathrm{aq}}^{\alpha/\beta}} &= \frac{\partial \left(\frac{\left(\Delta\omega^{\alpha/\beta}\right)^2 \mathrm{Prob}_{\mathrm{Emul,eq}} (1 - \mathrm{Prob}_{\mathrm{Emul,eq}})^2}{\left(\pi\Delta\nu_{\frac{1}{2},\mathrm{obs}}^{\alpha/\beta} - \left\langle \frac{1}{T_2^{*,\alpha/\beta}} \right\rangle\right)} \right)}{\partial \omega_{\mathrm{aq}}^{\alpha/\beta}} \\
&= \frac{k_B (\mathrm{Prob}_{\mathrm{Emul,eq}} - 1)}{\Delta\omega^{\alpha/\beta}} \left(\frac{1}{\mathrm{Prob}_{\mathrm{Emul,eq}}} - \frac{T_{2,\mathrm{exch}}}{T_{2\Delta}} \right)
\end{aligned} \tag{S14}$$

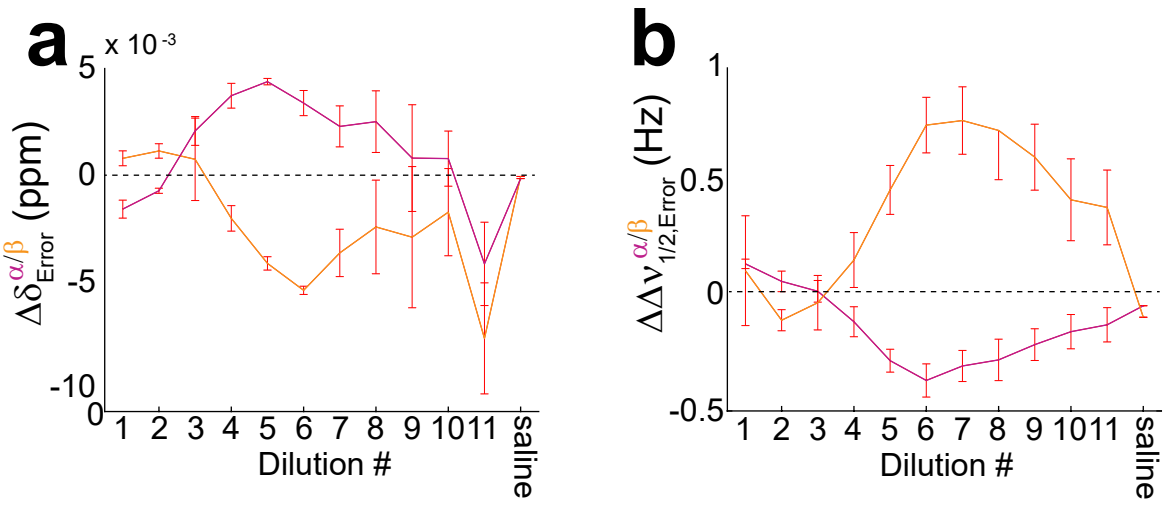

FIG. S3. The difference between the experimental and theoretical (calculated using the Bloch-McConnell equations with k_F and k_B given in Fig. 4 in the main manuscript) **a**) chemical shifts, $\Delta\delta^{\alpha/\beta}_{\text{Error}} = \delta^{\alpha/\beta}_{\text{obs}} - \delta^{\alpha/\beta}_{\text{theor.}}$, and **b**) line widths, $\Delta\Delta\nu_{\frac{1}{2}} = \Delta\nu^{\alpha/\beta}_{\frac{1}{2},\text{obs}} - \Delta\nu^{\alpha/\beta}_{\frac{1}{2},\text{theor.}}$, for the (magenta) H^{α} and (orange) H^{β} resonances. The dashed, horizontal lines denote $\Delta\delta^{\alpha/\beta}_{\text{Error}} = 0$ and $\Delta\Delta\nu^{\alpha/\beta}_{\frac{1}{2},\text{Error}} = 0$, and the error bars represent $\pm$ a standard deviation over three replicates.

Since the change in k_F and k_B due to changing $\omega^{\alpha/\beta}_{\text{aq}}$ to $\omega^{\alpha/\beta}_{\text{aq}} + \delta\omega^{\alpha/\beta}_{\text{aq}}$ is given by $\delta k_{F(B)} \approx \frac{\partial k_{F(B)}}{\partial \omega^{\alpha/\beta}_{\text{aq}}}\delta\omega^{\alpha/\beta}_{\text{aq}}$, the relative uncertainties in k_F and k_B due to uncertainties in $\omega^{\alpha/\beta}_{\text{aq}}$ are given by:

$$\begin{aligned}
\frac{\delta k_F}{k_F} &\approx \frac{\delta\omega^{\alpha/\beta}_{\text{aq}}}{\Delta\omega^{\alpha/\beta}}\left(1 - \frac{2}{\text{Prob}_{\text{Emul,eq}}} + (1 - \text{Prob}_{\text{Emul,eq}})\frac{T_{2,\text{exch}}}{T_{2\Delta}}\right) = m_{k_F,\omega_{aq}}\frac{\delta\omega^{\alpha/\beta}_{aq}}{\Delta\omega^{\alpha/\beta}} \\
\frac{\delta k_B}{k_B} &\approx \frac{\delta\omega^{\alpha/\beta}_{\text{aq}}}{\Delta\omega^{\alpha/\beta}}(\text{Prob}_{\text{Emul,eq}} - 1)\left(\frac{1}{\text{Prob}_{\text{Emul,eq}}} - \frac{T_{2,\text{exch}}}{T_{2\Delta}}\right) = m_{k_B,\omega_{aq}}\frac{\delta\omega^{\alpha/\beta}_{aq}}{\Delta\omega^{\alpha/\beta}}
\end{aligned} \tag{S15}$$

In Fig. S3**a** (left), both $m_{k_F,\omega_{\text{aq}}}$ and $m_{k_B,\omega_{\text{aq}}}$ in Eq. (S15) are plotted for dilutions $2-11$. In this case, both k_F and k_B were relatively insensitive to uncertainties in $\omega^{\alpha/\beta}_{\text{aq}}$ for low dilutions since $\text{Prob}_{\text{Emul,eq}}([\text{Emul}]) > 0.5$ for dilutions $1-4$. However, as $\text{Prob}_{\text{aq,eq}}([\text{Emul}]) \to 1$ with increasing dilution, the relative error in k_F and k_B became more sensitive to any uncertainty in $\omega^{\alpha/\beta}_{\text{aq}}$. In Fig. S3**a** (right), the upper bounds for $|\delta\nu_{\text{aq}}| = \left|\frac{\delta\omega_{\text{aq}}}{2\pi}\right|$ such that $\left|\frac{\Delta k_F}{k_F}\right| \leq 0.1$ and $\left|\frac{\Delta k_B}{k_B}\right| \leq 0.1$ are given. In this case, for dilutions $9-11$, $|\delta\nu_{\text{aq}}|$ ranged from 0.9 Hz down to 0.38 Hz in order that $\left|\frac{\Delta k_F}{k_F}\right| \leq 0.1$ while k_B was a bit more robust to uncertainties in ω_{aq} with $|\delta\nu_{\text{aq}}|$ ranging from 1.9 Hz down to 0.8 Hz.

For changes with respect to $\omega_{\text{Emul}}^{\alpha/\beta}$:

$$\begin{aligned}
\frac{\partial k_F}{\partial \omega_{\text{Emul}}^{\alpha/\beta}} &= \frac{\partial \left(\frac{\left(\Delta\omega^{\alpha/\beta}\right)^2 \text{Prob}_{\text{Emul,eq}}^2 (1-\text{Prob}_{\text{Emul,eq}})}{[\text{Emul}]\left(\pi\Delta\nu_{\frac{1}{2},\text{obs}}^{\alpha/\beta} - \left\langle \frac{1}{T_2^{\alpha/\beta}} \right\rangle\right)} \right)}{\partial \omega_{\text{Emul}}^{\alpha/\beta}} \\
&= \frac{k_F}{\Delta\omega^{\alpha/\beta}} \left(\frac{\text{Prob}_{\text{Emul,eq}}}{1-\text{Prob}_{\text{Emul,eq}}} + \text{Prob}_{\text{Emul,eq}} \frac{T_{2,\text{exch}}}{T_{2\Delta}} \right) \\
\frac{\partial k_B}{\partial \omega_{\text{Emul}}^{\alpha/\beta}} &= \frac{\partial \left(\frac{\left(\Delta\omega^{\alpha/\beta}\right)^2 \text{Prob}_{\text{Emul,eq}} (1-\text{Prob}_{\text{Emul,eq}})^2}{\left(\pi\Delta\nu_{\frac{1}{2},\text{obs}}^{\alpha/\beta} - \left\langle \frac{1}{T_2^{\alpha/\beta}} \right\rangle\right)} \right)}{\partial \omega_{\text{Emul}}^{\alpha/\beta}} \\
&= \frac{k_B}{\Delta\omega^{\alpha/\beta}} \left(\frac{1+\text{Prob}_{\text{Emul,eq}}}{1-\text{Prob}_{\text{Emul,eq}}} + \text{Prob}_{\text{Emul,eq}} \frac{T_{2,\text{exch}}}{T_{2\Delta}} \right)
\end{aligned} \tag{S16}$$

Since the change in k_F and k_B due to a small change in ω_{Emul} of $\delta\omega_{\text{Emul}}^{\alpha/\beta}$ is given by $\delta k_{F(B)} \approx \frac{\partial k_{F(B)}}{\partial \omega_{\text{Emul}}^{\alpha/\beta}} \delta\omega_{\text{Emul}}^{\alpha/\beta}$, the relative uncertainties in k_F and k_B due to uncertainties in $\omega_{\text{Emul}}^{\alpha/\beta}$ are given by:

$$\begin{aligned}
\frac{\delta k_F}{k_F} &\approx \frac{\delta\omega_{\text{Emul}}^{\alpha/\beta}}{\Delta\omega^{\alpha/\beta}} \left(\frac{\text{Prob}_{\text{Emul,eq}}}{1-\text{Prob}_{\text{Emul,eq}}} + \text{Prob}_{\text{Emul,eq}} \frac{T_{2,\text{exch}}}{T_{2\Delta}} \right) = m_{k_F,\omega_{\text{Emul}}} \frac{\delta\omega_{\text{Emul}}^{\alpha/\beta}}{\Delta\omega^{\alpha/\beta}} \\
\frac{\delta k_B}{k_B} &\approx \frac{\delta\omega_{\text{Emul}}^{\alpha/\beta}}{\Delta\omega^{\alpha/\beta}} \left(\frac{1+\text{Prob}_{\text{Emul,eq}}}{1-\text{Prob}_{\text{Emul,eq}}} + \text{Prob}_{\text{Emul,eq}} \frac{T_{2,\text{exch}}}{T_{2\Delta}} \right) = m_{k_B,\omega_{\text{Emul}}} \frac{\delta\omega_{\text{Emul}}^{\alpha/\beta}}{\Delta\omega^{\alpha/\beta}}
\end{aligned} \tag{S17}$$

In Fig. S3**b** (left), both $m_{k_F,\omega_{\text{Emul}}}$ and $m_{k_B,\omega_{\text{Emul}}}$ are plotted for dilutions $2-11$. In this case, both k_F and k_B were relatively sensitive to uncertainties in $\omega_{\text{Emul}}^{\alpha/\beta}$ at low dilutions since $\text{Prob}_{\text{Emul,eq}}([\text{Emul}]) > 0.5$ for dilutions 1-4. However, $\text{Prob}_{\text{aq,eq}}([\text{Emul}]) \to 0$ and hence $\frac{\Delta k_F}{k_F} \to 0$ and $\frac{\Delta k_B}{k_B} \to 0$ with increasing dilution. In Fig. S3**b** (right), the upper bounds for $|\delta\nu_{\text{Emul}}|$ such that $\left|\frac{\Delta k_F}{k_F}\right| \leq 0.1$ and $\left|\frac{\Delta k_B}{k_B}\right| \leq 0.1$ are given. In this case, k_F and k_B were somewhat insensitive to $\delta\nu_{\text{Emul}}$ except for dilution 2, where $|\delta\nu_{\text{Emul}}| < 0.5$ Hz or $\delta\nu_{\text{Emul}} < 1.1$ Hz in order that $\left|\frac{\Delta k_F}{k_F}\right| \leq 0.1$ and $\left|\frac{\Delta k_B}{k_B}\right| \leq 0.1$, respectively. The results in Fig. S3**b** also help to explain why the models where $\delta_{\text{Emul}}^{\alpha/\beta}$ were either fixed [Fig. S7] or changed with composition [Fig. 4 in the main text] gave similar results for k_F and k_B.

Finally, for changes with respect to $\left\langle \frac{1}{T_2^{*,\alpha/\beta}} \right\rangle$:

$$\frac{\partial k_F}{\partial \left\langle \frac{1}{T_2^{*,\alpha/\beta}} \right\rangle} = -\pi \frac{\partial k_F}{\partial \Delta\nu^{\alpha/\beta}_{\frac{1}{2},\text{obs}}} = \frac{k_F}{\pi\Delta\nu^{\alpha/\beta}_{\frac{1}{2},\text{obs}} - \left\langle \frac{1}{T_2^{*,\alpha/\beta}} \right\rangle} = k_F T_{2,\text{exch}}$$
$$\frac{\partial k_B}{\partial \left\langle \frac{1}{T_2^{*,\alpha/\beta}} \right\rangle} = -\pi \frac{\partial k_B}{\partial \Delta\nu^{\alpha/\beta}_{\frac{1}{2},\text{obs}}} = \frac{k_B}{\pi\Delta\nu^{\alpha/\beta}_{\frac{1}{2},\text{obs}} - \left\langle \frac{1}{T_2^{*,\alpha/\beta}} \right\rangle} = k_B T_{2,\text{exch}} \tag{S18}$$

Since the change in k_F and k_B to a small change in $\left\langle \frac{1}{T_2^{*,\alpha/\beta}} \right\rangle$ of $\delta \left\langle \frac{1}{T_2^{*,\alpha/\beta}} \right\rangle$ is given by $\delta k_{F(B)} \approx \frac{\partial k_{F(B)}}{\partial \left\langle \frac{1}{T_2^{*\alpha/\beta}} \right\rangle} \delta \left\langle \frac{1}{T_2^{*,\alpha/\beta}} \right\rangle$, the uncertainties in k_F and k_B are given by:

$$\left|\frac{\Delta k_F}{k_F}\right| = \left|\frac{\Delta k_B}{k_B}\right| \approx T_{2,\text{exch}} \left|\delta \left\langle \frac{1}{T_2^{*,\alpha/\beta}} \right\rangle\right| = \pi T_{2,\text{exch}} \frac{1}{\pi} \left|\delta \left\langle \frac{1}{T_2^{*,\alpha/\beta}} \right\rangle\right|$$
$$= \pi T_{2,\text{exch}} \left|\delta\Delta\nu^{\alpha/\beta}_{\frac{1}{2}}\right| = m_{k_{F(B)},\delta\Delta\nu_{\frac{1}{2}}} \left|\delta\Delta\nu^{\alpha/\beta}_{\frac{1}{2}}\right| \tag{S19}$$

From Eq. (S19), the relative uncertainties in k_F and k_B are identical and inversely proportional to the exchange broadening, $\frac{1}{\pi T_{2,\text{exch}}} = \frac{\left(\Delta\omega^{\alpha/\beta}\right)^2 \text{Prob}_{\text{Emul,eq}}(1-\text{Prob}_{\text{Emul,eq}})}{k_{\text{exch}}}$. This suggests that k_F and k_B are both sensitive to uncertainties in either line widths or changes to the intrinsic T_2^*s at low and high dilutions, i.e., where there is little exchange broadening. This is shown more clearly in Fig. S3**c**, where the uncertainties in the observed line width and/or the intrinsic T_2^* broadening such that $\left|\frac{\Delta k_F}{k_F}\right| = \left|\frac{\Delta k_B}{k_B}\right| \leq 0.1$, ranged between 0.05 Hz (for dilution 2) to 0.92 Hz for the H^β resonance and between 0.06 Hz (for dilution 2) to 1.78 Hz for the H^α resonance.

C. Residual dipolar couplings

We now wish to explicitly consider the effects of residual dipolar couplings (*RDC*s) on the observed splitting and line widths. It is known[1] that in the fast exchange regime, *RDC*s can lead to differences in line broadening within a multiplet. During the course of dilution, the individual peaks within the H^α quartet cannot be resolved except in the first dilutions and in saline. Furthermore, the H^α resonance overlapped with the upfield peak of the H^β multiplet starting at the third dilution. However, the downfield and middle peaks of the H^β multiplet were always well resolved over all dilutions as shown in Fig. 3 in the main text.

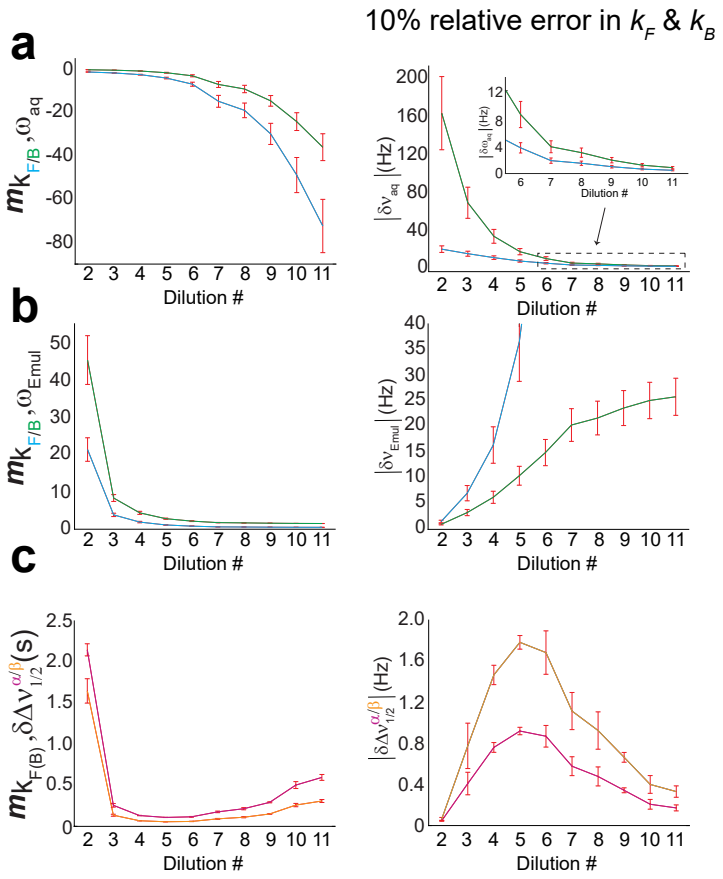

FIG. S4. Plots of the relevant tolerances of k_F and k_B (given in Fig. 4 of the main text and Table II) on **a**) $\nu_{\rm aq}^{\alpha/\beta}$, **b**) $\nu_{\rm Emul}^{\alpha/\beta}$, and **c**) $\Delta\nu_{\frac{1}{2}}^{\alpha/\beta}$. In **a**) both (blue) $m_{k_F,\rm aq}$ and (green) $m_{k_B,\rm aq}$ in Eq. (S15) are plotted on the left for dilutions $2-11$ while the corresponding upper limits to the uncertainties in $\nu_{\rm aq}$, $|\delta\nu_{aq}|$, such that (blue) $\left|\frac{\Delta k_F}{k_F}\right| \leq 0.1$ and (green) $\left|\frac{\Delta k_B}{k_B}\right| \leq 0.1$ are plotted on the right. In **b**), both (blue) $m_{k_F,\rm Emul}$ and (green) $m_{k_B,\rm Emul}$ in Eq. (S17) are plotted on the left for dilutions $2-11$ while the corresponding upper limits to the uncertainties in $\nu_{\rm Emul}$, $|\delta\nu_{Emul}|$, such that (blue) $\left|\frac{\Delta k_F}{k_F}\right| \leq 0.1$ and (green) $\left|\frac{\Delta k_B}{k_B}\right| \leq 0.1$. In **a** and **b**, the error bars represent $\pm$ a standard deviation after averaging over both $\mathrm{H}^{\alpha/\beta}$ resonances in three replicates. In **c**, both (magenta) $m_{F(B),\delta\Delta\nu_{\frac{1}{2}}^{\alpha}}$ and (orange) $m_{F(B),\delta\Delta\nu_{\frac{1}{2}}^{\beta}}$ from Eq. (S19) are plotted for dilutions $2-11$ on the left while the corresponding upper bounds for the absolute uncertainties for (magenta) $\left|\delta\Delta\nu_{\frac{1}{2}}^{\alpha}\right|$ and (orange) $\left|\delta\Delta\nu_{\frac{1}{2}}^{\beta}\right|$ such that $\left|\frac{\Delta k_F}{k_F}\right| \leq 0.1$ and $\left|\frac{\Delta k_B}{k_B}\right| \leq 0.1$ given on the right. In **c**, the error bars represent $\pm$ a standard deviation averaged over three replicates.

As such, only the H^β resonance will be considered in assessing the importance of RDCs on the dilution spectra of the system studied in this work.

The Hamiltonian for the H^β spin within an emulsion droplet can be written as:

$$\frac{\widehat{H}^{\beta}_{\text{Emul}}}{\hbar} = \omega^{\beta}_{\text{Emul}}\widehat{I}_Z + 2\pi\tilde{J}_{1,\text{Emul}}\widehat{I}_Z\widehat{S}_{Z1} + 2\pi\tilde{J}_{2,\text{Emul}}\widehat{I}_Z\widehat{S}_{Z2} \tag{S20}$$

where $\tilde{J}_{1,\text{Emul}} = J^{\beta}_{1,\text{Emul}} + RDC_{\text{Emul}}$ and $\tilde{J}_{2,\text{Emul}} = J^{\beta}_{2,\text{Emul}} + RDC_{\text{Emul}}$ are the effective coupling strengths in the emulsion, which includes the spin-spin scalar couplings and any RDCs that are present (spin-spin couplings between the fluorine atoms are assumed to still be in the weak-coupling limit and as such are not included in Eq. (S20)).

The Hamiltonian for the H^β spin within the aqueous phase can be written as:

$$\frac{\widehat{H}^{\beta}_{\text{aq}}}{\hbar} = \omega^{\beta}_{\text{aq}}\widehat{I}_Z + 2\pi\tilde{J}_{\text{aq}}\left(\widehat{S}_{Z1} + \widehat{S}_{Z2}\right)\widehat{I}_Z \tag{S21}$$

where $\tilde{J}_{\text{aq}} = J^{\beta}_{\text{aq}} + RDC_{\text{aq}}$. From Table 1 in the main manuscript, $J^{\beta}_{\text{aq}} = 71.1$ Hz, $J^{\beta}_{1,\text{Emul}} = 70.3$ Hz, and $J^{\beta}_{2,\text{Emul}} = 72.2$ Hz. As written in Eq. (S20) and Eq. (S21), the H^β resonance will appear as a doublet of doublets in the emulsion droplet for $\tilde{J}_{1,\text{Emul}} \neq \tilde{J}_{2,\text{Emul}}$ and as a triplet in the aqueous phase.

The expected frequencies and line widths in the fast-exchange regime for the downfield and middle peaks of the H^β multiplet depend upon the frequency differences between the organic and aqueous phases of the corresponding transitions, which are given by:

$$\begin{aligned}
\Delta\omega^{\beta}_{\downarrow\downarrow} &= \Delta\omega^{\beta} + \Delta\tilde{J}^{\beta}_{\downarrow\downarrow} = \Delta\omega^{\beta} + 2\pi\left(\frac{\tilde{J}_{1,\text{Emul}} + \tilde{J}_{2,\text{Emul}}}{2} - \tilde{J}_{\text{aq}}\right) \\
&= \Delta\omega^{\beta} + 2\pi\left(\Delta J^{\beta} + \Delta RDC^{\beta}\right) \\
\Delta\omega^{\beta}_{\uparrow\downarrow} &= \Delta\omega^{\beta} + \Delta\tilde{J}^{\beta}_{\uparrow\downarrow} = \Delta\omega^{\beta} + 2\pi\frac{\left(\tilde{J}_{2,\text{Emul}} - \tilde{J}_{1,\text{Emul}}\right)}{2} \\
&= \Delta\omega^{\beta} + 2\pi\Delta J^{\beta}_{12} \\
\Delta\omega^{\beta}_{\downarrow\uparrow} &= \Delta\omega^{\beta} - \Delta\tilde{J}^{\beta}_{\uparrow\downarrow} = \Delta\omega^{\beta} - 2\pi\frac{\left(\tilde{J}_{2,\text{Emul}} - \tilde{J}_{1,\text{Emul}}\right)}{2} \\
&= \Delta\omega^{\beta} - 2\pi\Delta J^{\beta}_{12}
\end{aligned} \tag{S22}$$

where the subscripts denotes the corresponding spin states of the fluorine nuclei, $\Delta\omega^{\beta} = \omega^{\beta}_{\text{Emul}} - \omega^{\beta}_{\text{aq}}$, $\Delta J^{\beta} = \frac{J_{1,\text{Emul}} + J_{2,\text{Emul},2}}{2} - J_{\text{aq}} = 0.154$ Hz, $\Delta RDC^{\beta} = RDC_{\text{Emul}} - RDC_{\text{aq}}$, and $\Delta J^{\beta}_{12} = \frac{J_{2,\text{Emul}} - J_{1,\text{Emul}}}{2} = 0.95$ Hz.

The predicted frequencies for the downfield ($\omega^{\beta}_{\mathrm{obs},\downarrow\downarrow}$) and middle peaks ($\omega^{\beta}_{\mathrm{obs},\uparrow\downarrow}$ and $\omega^{\beta}_{\mathrm{obs},\downarrow\uparrow}$) are given by:

$$\begin{aligned}
\omega^{\beta}_{\mathrm{obs},\downarrow\downarrow} &= \omega^{\beta}_{aq} + 2\pi\tilde{J}_{aq} + \mathrm{Prob}_{\mathrm{Emul,eq}}([\mathrm{Emul}])\Delta\omega^{\beta}_{\downarrow\downarrow} \\
\omega^{\beta}_{\mathrm{obs},\uparrow\downarrow} &= \omega^{\beta}_{\mathrm{aq}} + \mathrm{Prob}_{\mathrm{Emul,eq}}([\mathrm{Emul}])\Delta\omega^{\beta}_{\uparrow\downarrow} \\
\omega^{\beta}_{\mathrm{obs},\downarrow\uparrow} &= \omega^{\beta}_{\mathrm{aq}} + \mathrm{Prob}_{\mathrm{Emul,eq}}([\mathrm{Emul}])\Delta\omega^{\beta}_{\downarrow\uparrow}
\end{aligned}$$

When $\omega^{\beta}_{\mathrm{obs},\uparrow\downarrow}$ and $\omega^{\beta}_{\mathrm{obs},\downarrow\uparrow}$ can be resolved (as illustrated shown in Fig. S5**a** (left)), the effective observed splittings in the fast-exchange regime are given by:

$$\begin{aligned}
J^{\beta}_{\mathrm{obs},1} = \frac{\omega^{\beta}_{\mathrm{obs}\downarrow\downarrow} - \omega^{\beta}_{\mathrm{obs},\uparrow\downarrow}}{2\pi} &= \tilde{J}_{\mathrm{aq}} + \mathrm{Prob}_{\mathrm{Emul,eq}}([\mathrm{Emul}])\left(\frac{\Delta\omega^{\beta}_{\downarrow\downarrow} - \Delta\omega^{\beta}_{\uparrow\downarrow}}{2\pi}\right) \\
&= J_{\mathrm{aq}} + RDC_{\mathrm{aq}} + \mathrm{Prob}_{\mathrm{Emul,eq}}([\mathrm{Emul}])\left(\Delta J^{\beta} - \Delta J^{\beta}_{12} + \Delta RDC^{\beta}\right) \\
J^{\beta}_{\mathrm{obs},2} = \frac{\omega^{\beta}_{\mathrm{obs}\downarrow\downarrow} - \omega^{\beta}_{\mathrm{obs},\downarrow\uparrow}}{2\pi} &= \tilde{J}_{\mathrm{aq}} + \mathrm{Prob}_{\mathrm{Emul,eq}}([\mathrm{Emul}])\left(\frac{\Delta\omega^{\beta}_{\downarrow\downarrow} - \Delta\omega^{\beta}_{\downarrow\uparrow}}{2\pi}\right) \\
&= J_{\mathrm{aq}} + RDC_{\mathrm{aq}} + \mathrm{Prob}_{\mathrm{Emul,eq}}([\mathrm{Emul}])\left(\Delta J^{\beta} + \Delta J^{\beta}_{12} + \Delta RDC^{\beta}\right)
\end{aligned} \tag{S23}$$

For the third dilution and higher, $\omega^{\beta}_{\mathrm{obs},\uparrow\downarrow}$ and $\omega^{\beta}_{\mathrm{obs},\downarrow\uparrow}$ cannot be resolved, and thus an average effective splitting is measured as illustrated in Fig. S5**a** (right), which can be approximated by:

$$\begin{aligned}
J^{\beta}_{obs} &= \frac{J^{\beta}_{\mathrm{obs},1} + J^{\beta}_{\mathrm{obs},2}}{2} \\
&= J_{\mathrm{aq}} + RDC_{\mathrm{aq}} + \mathrm{Prob}_{\mathrm{Emul,eq}}([\mathrm{Emul}])\left(\Delta J^{\beta} + \Delta RDC^{\beta}\right)
\end{aligned} \tag{S24}$$

In this case, J^{β}_{obs} is expected to depend linearly on $\mathrm{Prob}_{\mathrm{Emul,eq}}$ (assuming that ΔRDC^{β} does not change with dilution). The experimentally observed values for $J^{\beta}_{\mathrm{obs},1}$ and $J^{\beta}_{\mathrm{obs},2}$ for the first two dilutions and J^{β}_{obs} for dilutions $3-11$ are given in Fig. S5**b**.

In Fig. S5**c**, the experimentally observed J^{β}_{obs} for dilutions $3-11$ are plotted versus $\mathrm{Prob}_{\mathrm{Emul,eq}}$ along with the best fit to Eq. (S24) (solid, green line). From the best fit, $RDC_{\mathrm{aq}} \approx (0.046 \pm 0.014)$ Hz, $\Delta RDC^{\beta} \approx -(0.003 \pm 0.04)$ Hz, and $RDC_{\mathrm{Emul}} = \Delta RDC^{\beta} + RDC_{\mathrm{aq}} = (0.043 \pm 0.054)$ Hz. A linear dependence of J^{β}_{obs} vs. $\mathrm{Prob}_{\mathrm{Emul,eq}}$ in Eq. (S24) was only expected if the RDCs did not change with dilution. However, RDC_{aq} would be expected to decrease and eventually disappear with increasing dilution. With that in

mind, a linear fit for dilutions three and four is also shown (dashed, yellow line), which gave $\Delta RDC^{\beta} = 0.289$ Hz, $RDC_{\text{aq}} = -0.154$ Hz, $RDC_{\text{Emul}} = 0.135$ Hz. In any case, RDCs, if present, are expected to be less than 0.5 Hz based upon the observed splitting in the H^{β} multiplet.

While the effect of RDCs on J^{β}_{obs} do not ultimately affect the determination of k_F and k_B, RDCs can alter the line widths that are used to determine k_F and k_B [Eq. (15) in the main text]. In this case, the predicted line widths in the fast-exchange regime for the middle and downfield resonances of the H^{β} multiplet are given by:

$$\begin{aligned}
\Delta\nu^{\beta}_{\frac{1}{2},\downarrow\downarrow} &= \Delta\nu^{\beta}_{\frac{1}{2},\downarrow\downarrow,\text{intrinsic}} + \frac{\left(\Delta\omega^{\beta}_{\downarrow\downarrow}\right)^2 \text{Prob}_{\text{Emul,eq}}\left(1-\text{Prob}_{\text{Emul,eq}}\right)}{\pi k_{\text{exch}}} \\
\Delta\nu^{\beta}_{\frac{1}{2},\uparrow\downarrow} &= \Delta\nu^{\beta}_{\frac{1}{2},\uparrow\downarrow,\text{intrinsic}} + \frac{\left(\Delta\omega^{\beta}_{\uparrow\downarrow}\right)^2 \text{Prob}_{\text{Emul,eq}}\left(1-\text{Prob}_{\text{Emul,eq}}\right)}{\pi k_{\text{exch}}} \\
\Delta\nu^{\beta}_{\frac{1}{2},\downarrow\uparrow} &= \Delta\nu^{\beta}_{\frac{1}{2},\downarrow\uparrow,\text{intrinsic}} + \frac{\left(\Delta\omega^{\beta}_{\downarrow\uparrow}\right)^2 \text{Prob}_{\text{Emul,eq}}\left(1-\text{Prob}_{\text{Emul,eq}}\right)}{\pi k_{\text{exch}}}
\end{aligned} \tag{S25}$$

Since $\Delta\omega^{\beta}_{\downarrow\downarrow} \neq \Delta\omega^{\beta}_{\uparrow\downarrow} \neq \Delta\omega^{\beta}_{\downarrow\uparrow}$, from Eq. (S25) we would expect that $\Delta\nu^{\beta}_{\frac{1}{2},\downarrow\downarrow} \neq \Delta\nu^{\beta}_{\frac{1}{2},\uparrow\downarrow} \neq \Delta\nu^{\beta}_{\frac{1}{2},\downarrow\uparrow}$. In Fig. S6**a**, the observed line widths for the (green) middle and (blue) downfield peaks of the H^{β} multiplet from the dilution spectra in Fig. 3 of the main manuscript are shown. With the exception of dilutions 5-7, the line widths were nearly identical within the uncertainty of the measurements as shown in Fig. S6**b**. The differences in line widths, $\Delta\Delta\nu^{\beta}_{\frac{1}{2}} = \Delta\nu^{\beta}_{\frac{1}{2},\uparrow\downarrow/\downarrow\uparrow} - \Delta\nu^{\beta}_{\frac{1}{2},\downarrow\downarrow}$ were $\Delta\Delta\nu^{\beta}_{\frac{1}{2}} = (0.4 \pm 0.2)$ Hz, $\Delta\Delta\nu^{\beta}_{\frac{1}{2}} = (0.6 \pm 0.2)$ Hz, and $\Delta\Delta\nu^{\beta}_{\frac{1}{2}} = (0.2 \pm 0.1)$ Hz for dilutions 5, 6, and 7, respectively. Since $\Delta\nu^{\beta} \approx 200$ Hz, a deviation caused by RDCs of 1 Hz would only change the line width by approximately 1.1%. Furthermore, the possible errors or uncertainties in line widths in dilutions 5-7 mainly occurred when the exchange broadening was largest, i.e., when the NMR-determined k_F and k_B values were the least sensitive to these uncertainties [Fig. S3**c**]. As such, the presence of RDCs in the isoflurane/FC43 emulsion, if present, do not appear to significantly impact the NMR-determined rate constants.

D. Determination of k_F and k_B for fixed $\delta^{\alpha}_{\text{Emul}}$ and $\delta^{\beta}_{\text{Emul}}$

Instead of modeling $\delta^{\alpha/\beta}_{\text{Emul}}$ to change with $\phi^{\text{Org}}_{\text{Iso}}$, k_F and k_B were also determined in the fast-exchange limit under the conditions of fixed $\delta^{\alpha/\beta}_{\text{Emul}}$, which were determined to be $\delta^{\alpha,\text{fixed}}_{\text{Emul}} =$

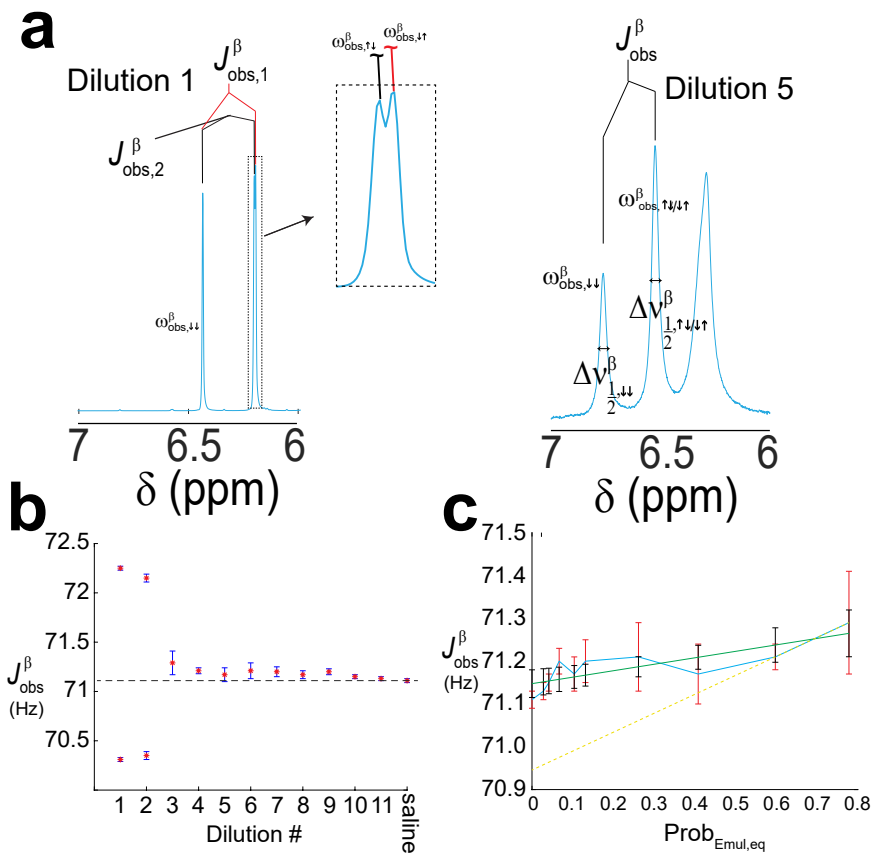

FIG. S5. The observed splitting between the middle and downfield resonances of the H$^\beta$ multiplet. **a**) In the emulsion phase, the H$^\beta$ resonance is a doublet of doublets, where $\omega^\beta_{\uparrow\downarrow}$ and $\omega^\beta_{\downarrow\uparrow}$ can only be resolved for the first two dilutions (left) whereas for dilution 3 and higher they were unresolved. **b**) A plot of $J^\beta_{\rm obs}$ for dilutions $1-11$ determined from the dilution spectra of a single replicate used in Fig. 3 of the main manuscript. The dashed line denotes $J^\beta_{\rm aq}$ in pure saline. Only for dilutions 1 and 2 are $J^\beta_{\rm obs,1}$ and $J^\beta_{\rm obs,2}$ resolved. The error bars represent $\pm$ a standard deviation (as determined using Topspin when measuring $J^\beta_{\rm obs}$). **c**) Plot of $J^\beta_{\rm obs}$ vs. Prob$_{\rm Emul,eq}$ for dilutions $3-11$ (blue curve). The red error bars represent $\pm$ a standard deviation (as determined using Topspin when measuring $J^\beta_{\rm obs}$). The best fit to Eq. (S24) (green line) is shown, which gave $J^\beta_{\rm aq} + RDC^\beta_{\rm aq} = (71.15 \pm 0.04)$ Hz and $\Delta J^\beta + \Delta RDC^\beta = (0.151 \pm 0.014)$ Hz. The black error bars represent the 95% confidence intervals associated with the best fit line. A fit using only dilution 3 (Prob$_{\rm Emul,eq} = 0.7783$) and dilution 4 (Prob$_{\rm Emul,eq} = 0.5975$) is also shown (yellow, dashed line) with $J^\beta_{\rm aq} + RDC^\beta_{\rm aq} = 70.95$ Hz and $\Delta J^\beta + \Delta RDC^\beta = 0.443$ Hz.

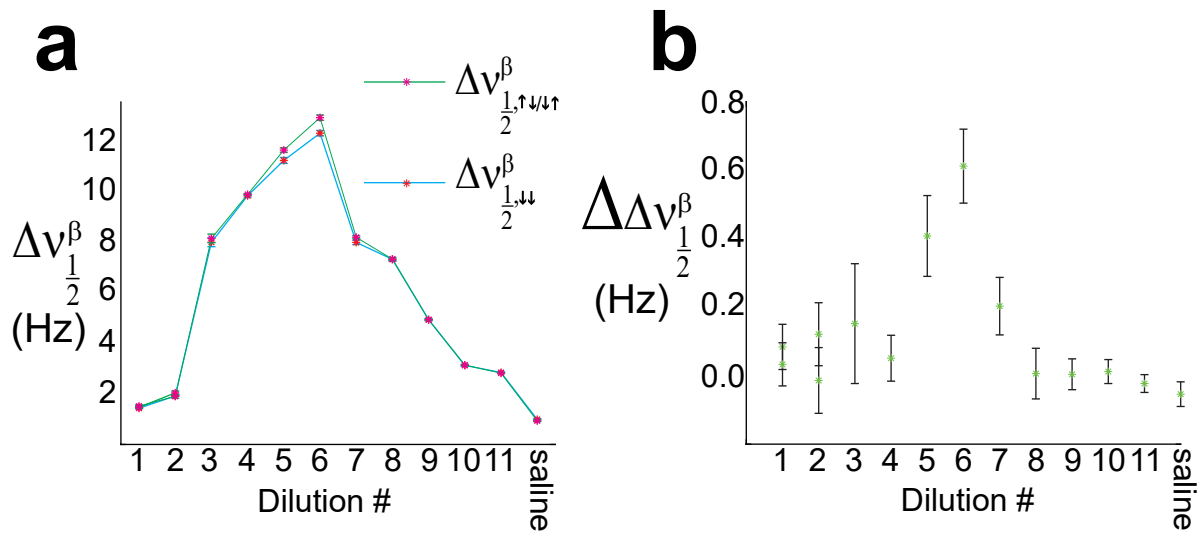

FIG. S6. **a**) Experimental line widths of the H^{β} multiplet taken from the dilution spectra in Fig. 3 in the main text. In this case, the line widths of the downfield ($\Delta\nu^{\beta}_{\frac{1}{2},\downarrow\downarrow}$, blue) and the middle peaks ($\Delta\nu^{\beta}_{\frac{1}{2},\uparrow\downarrow}$ and $\Delta\nu^{\beta}_{\frac{1}{2},\downarrow\uparrow}$ for dilutions 1 and 2 and $\Delta\nu^{\beta}_{\frac{1}{2},\uparrow\downarrow/\downarrow\uparrow}$ for dilutions 3-11 and in saline) are shown. The line widths were measured using Topspin, and the error bars represent ± a standard deviation as determined using Topspin when measuring $\nu^{\beta}_{\text{obs},\downarrow\downarrow}$ and $\nu^{\beta}_{\text{obs},\uparrow\downarrow/\downarrow\uparrow}$. **b**) The difference in line widths, $\Delta\Delta\nu^{\beta}_{\frac{1}{2}} = \Delta\nu^{\beta}_{\frac{1}{2},\uparrow\downarrow/\downarrow\uparrow} - \Delta\nu^{\beta}_{\frac{1}{2},\downarrow\downarrow}$.

5.83 ± 0.01 ppm and $\delta^{\beta,\text{fixed}}_{\text{Emul}} = 6.19 \pm 0.02$ ppm.

In this case, Eq. (15) was used to determine k_F and k_B at each [Emul], which are given in Fig. S7. Compared to Fig. 4 in the main text, the various k_F and k_B using either fixed or changing $\delta^{\alpha/\beta}_{\text{Emul}}$ were still on the same order of magnitude with each other although the first dilution shown in Fig. S7**b** had a k_F that was above the Smoluchowski diffusion limited bimolecular rate constant[2], k_{diff} given in Eq. (S26). The experimental and theoretical spectra for a series of dilution experiments are given in Fig. S8, which, as with Fig. 3 in the main text, were in general agreement. While kinetic parameters that were consistent with the experimental dilution spectra using either [Fig. S8] fixed or [Fig. 3 of main text] $\delta^{\alpha/\beta}_{\text{Emul}}\left(\phi^{\text{Org}}_{\text{Iso}}\right)$ could be found, the observed $[\text{Iso}]_{\text{tot}}$-dependence of the spectrum shown in Fig. 7 was inconsistent with the model using fixed chemical shifts in the emulsion phase.

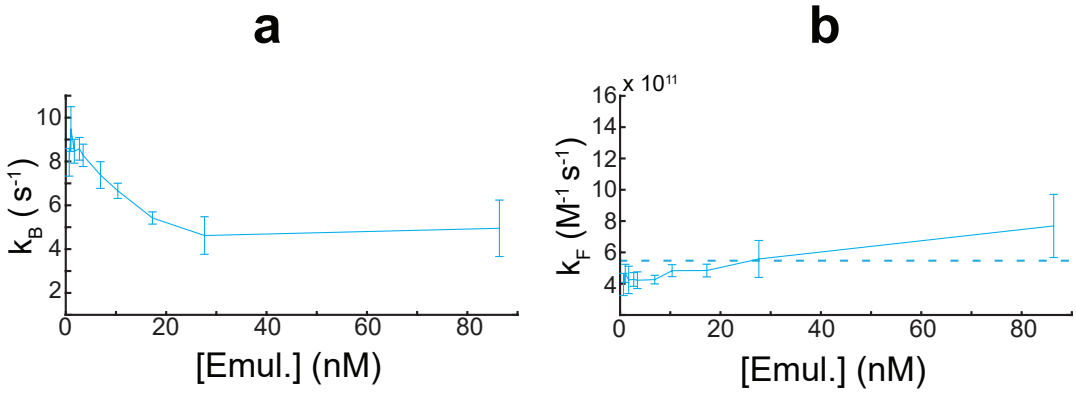

FIG. S7. The NMR determined rate constants, k_F and k_B in as a function of [Emul] using Eq. (15) in the main text with fixed $\delta^{\alpha/\beta}_{\text{Emul}}$. The error bars represent ± a standard deviation from averaging over the rate constants determined from both H^{α} and H^{β} resonances of isoflurane in three replicates. **a**) As [Emul] decreased, k_B increased by about a factor of two while k_F decreased by almost a factor of two in **b**. For the first two dilutions, k_F was above the corresponding diffusion-limited, Smoluchowski bimolecular rate constant, k_{diff} [Eq. (S26)], which is denoted by the dashed line.

II. ALTERNATIVE FITTING PROCEDURE

The fitting procedure described in the main text used formulas for both ν_{obs} and $\Delta\nu_{\frac{1}{2},\text{obs}}$ in the fast-exchange regime to determine k_B and k_F. An alternative fitting procedure was also used without making the assumption of fast-exchange in order to find the corresponding k_F and k_B that minimized the differences between the experimental spectra and the spectra calculated using the Bloch-McConnell equations in Eq. (S1) and Eq. (S7). This was accomplished using a simulated annealing method from the MATLAB Global Optimization Toolbox. The kinetic parameters were further minimized using the "fmincon" function, which provided the Hessian matrix that was used to determine the standard errors of the kinetic parameters in the fit. Furthermore, the minimization could be run while imposing constraints on the kinetic parameters (something that was not possible for the fitting procedure described in the main text, which simply found k_B and k_F using algebraic manipulation of the observed line widths and shifts). In the following we will present two models that were investigated: (A) fixed k_F, k_B, and $\delta^{\alpha/\beta}_{\text{Emul}}$, and (B) fixed k_B and $\delta^{\alpha/\beta}_{\text{Emul}}$. It should be noted that since $\delta^{\alpha/\beta}_{\text{Emul}}$ is fixed in all of these models, all of these models would be inconsistent with the observed $[\text{Iso}]_{\text{tot}}$-dependence seen in Fig. 7 in the main text.

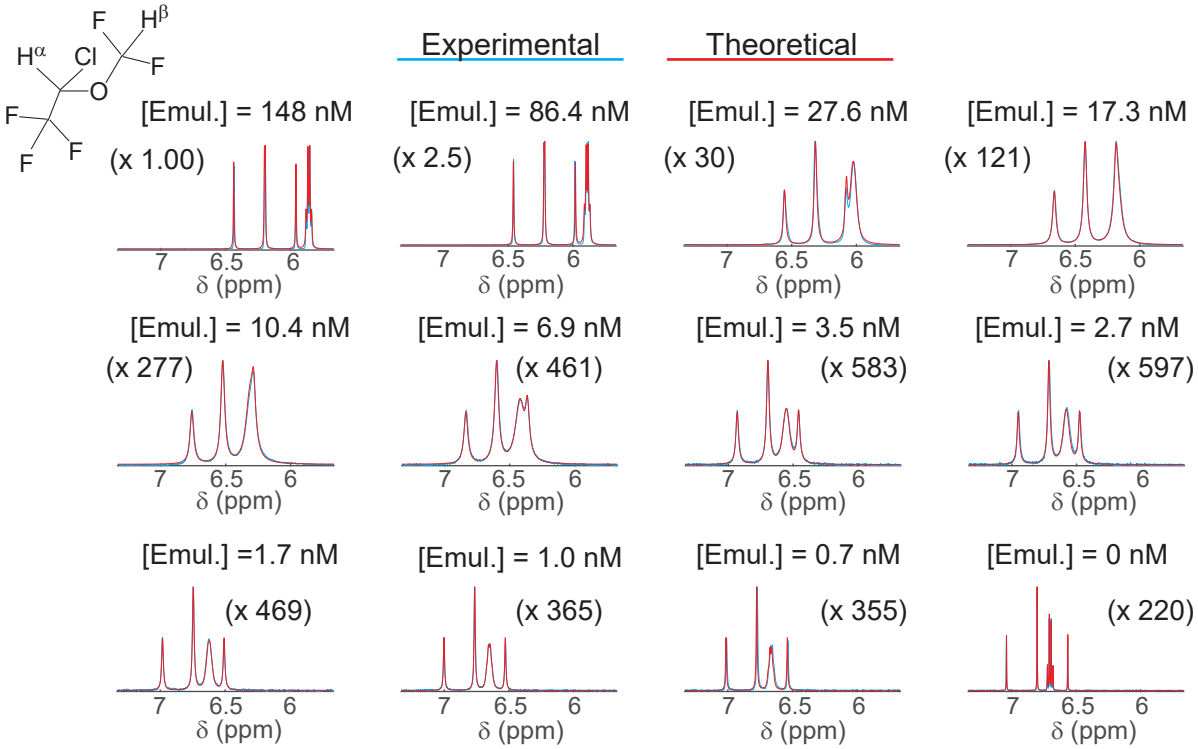

FIG. S8. (blue) Experimental and (red) theoretical [calculated from the Bloch-McConnell equations using fixed $\delta^{\alpha/\beta}_{\text{Emul}}$] ^{1}H-NMR spectra of isoflurane in an emulsion diluted in a series of experiments with varying [Emul]. Top Left: isoflurane in the emulsion; Bottom right: isoflurane dissolved in pure saline. The level of agreement between experiment and theory was similar to that found in Fig. 3 of the main text where $\delta^{\alpha/\beta}_{\text{Emul}}$ changed with $\phi^{\text{Org}}_{\text{Iso}}$ as given in Eqs. (S6) and (S11). Scaling factors relative to the initial isoflurane emulsion spectrum (top left) are shown.

A. Fixed k_F, k_B, and $\delta^{\alpha/\beta}_{\text{Emul}}$

In this case, k_B, k_F, and $\delta^{\alpha/\beta}_{\text{Emul}}$ were taken to be constant and independent of [Emul]. As shown in Fig. S9, fixing the kinetic parameters over the entire dilution range did not provide as good of a fit to the experimental dilution spectra as was found in Fig. 3 of the main manuscript where k_B, k_F, and $\delta^{\alpha/\beta}_{\text{Emul}}$ were allowed to change with [Emul]. However it should be noted that the optimal kinetic parameters were still on the same order of magnitude as was observed in Fig. 4 in the main manuscript: $k_B^{\text{fixed}} = 7220\,\text{s}^{-1}$ and $k_F^{\text{fixed}} = 9.669\times10^{11}\,\text{M}^{-1}\text{s}^{-1}$ for the emulsion.

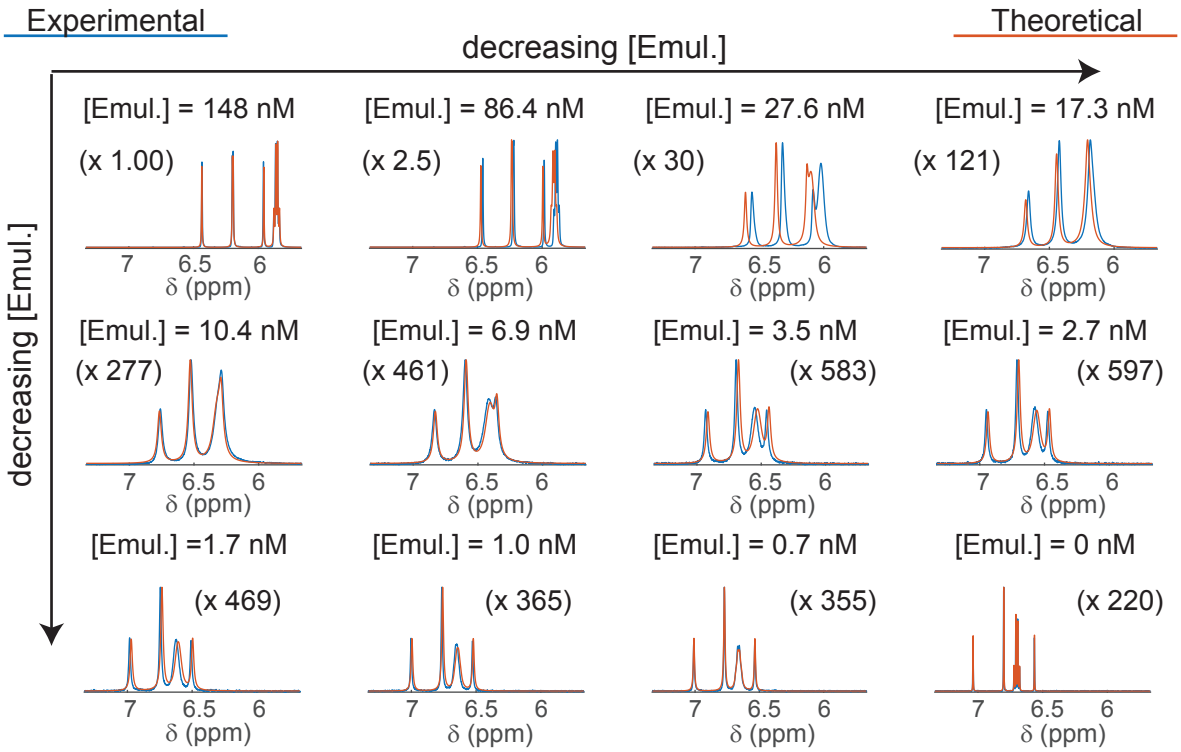

FIG. S9. (blue) Experimental and (red) theoretical (calculated using $k_F^{\text{fixed}} = 9.669 \times 10^{11}\,\text{M}^{-1}\text{s}^{-1}$ and $k_B^{\text{fixed}} = 7220\,\text{s}^{-1}$) ^{1}H-NMR spectra of isoflurane in an emulsion diluted in a series of experiments with varying [Emul] achieved by dilution with an isoflurane in D_2O saline solution. Top Left: isoflurane in the emulsion, Bottom right: isoflurane dissolved in pure saline. The fit using fixed k_F and k_B was not as good as that found in Fig. 3 of the main text, although k_F^{fixed} and k_B^{fixed} were still on the same order of magnitude as the k_F and k_B values found in Fig. 4 of the main text. The following parameters were used in the fit: $T_{2,\text{aq}}^{*,\alpha} = 0.35$ s, $T_{2,\text{aq}}^{*,\beta} = 0.4$ s, $T_{2,\text{Emul}}^{*,\alpha} = 0.4$ s, $T_{2,\text{Emul}}^{*,\beta} = 0.32$ s, $\delta_{\text{Emul}}^{\alpha} = 5.7728$ ppm, and $\delta_{\text{Emul}}^{\beta} = 6.1366$ ppm. Scaling factors relative to the initial isoflurane emulsion spectrum (top left) are shown.

B. Fixed k_B and $\delta_{\text{Emul}}^{\alpha/\beta}$

In this case, k_B and $\delta_{\text{Emul}}^{\alpha/\beta}$ were taken to be constant and independent of [Emul] while k_F was allowed to vary with [Emul]. Under these constraints, the chemical shifts of the isoflurane resonances in the emulsion were nearly identical, $\delta_{\text{Emul}}^{\alpha,\text{model}} = 6.22 \pm 0.01$ ppm and $\delta_{\text{Emul}}^{\beta,\text{model}} = 6.23 \pm 0.01$ ppm. As shown in Fig. S10, excellent agreement between the observed and theoretical spectra for the emulsion under a series of dilution experiments was obtained.

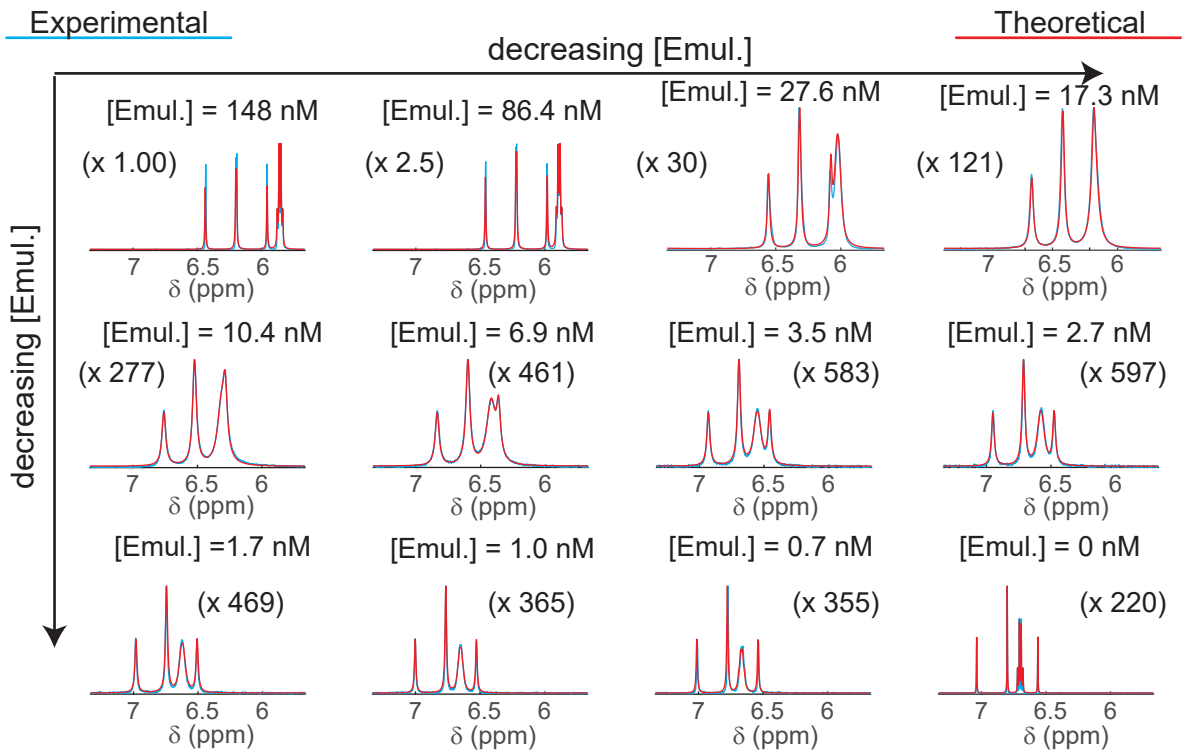

FIG. S10. (blue) Experimental and (red) calculated using fixed $k_B = (7122 \pm 13)\,\mathrm{s}^{-1}$ and $\delta^{\alpha/\beta}_{\mathrm{Emul}}$ with k_F given in Fig. S11 (blue, solid curve), the ^{1}H-NMR spectra of isoflurane in an emulsion diluted in a series of experiments with varying [Emul] achieved by dilution with an isoflurane saline solution. Top Left: Isoflurane in the emulsion, Bottom right: Isoflurane dissolved in pure saline. Scaling factors relative to the initial isoflurane emulsion spectrum (top left) are shown.

In Fig. S11, the corresponding values of k_F from this model were plotted (blue, solid curve) versus the volume fraction of the organic phase, $\phi_{\mathrm{Organic}} = \frac{4\pi}{3} r^3_{\mathrm{Emul}} N_A[\mathrm{Emul}]$ where N_A is Avogadro's number and r_{Emul} is the average radius of an emulsion droplet. For comparison, the NMR-determined k_F values from Fig. 4**b** from the main text (black, solid curve) are also plotted. These tended to be smaller than those for the model with fixed k_B for $\phi > 0.01$, after which it became smaller.

It should be noted that k_F's determined from both models were within an order of magnitude of each other and were within an order of magnitude of the theoretical Smoluchowski diffusion-limited rate constant[2] predicted for the emulsions:

$$k_{\mathrm{diff}} = 4\pi r_{\mathrm{Emul}} D_{Iso,\mathrm{saline}} N_A \tag{S26}$$

indicating that isoflurane entering the spherical emulsion was diffusion limited. Prior the-

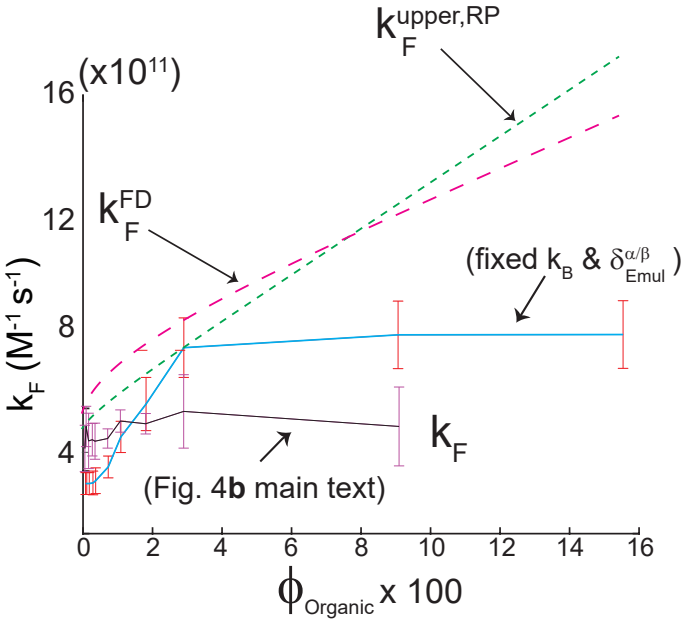

FIG. S11. The dependence of the (averaged over $n = 3$ replicates) forward rate constant, k_F, versus the organic phase volume fraction, ϕ_{Organic} for (blue, solid curve) fixed k_B and $\delta_{\text{Emul}}^{\alpha/\beta}$ and for (black solid curve) the case where $\delta_{\text{Emul}}^{\alpha/\beta}$ and k_B were alowed to change with [Emul], which were given in Fig. 4**b** in the main text. In general, the values of k_F for both models were on the same order of magnitude as the diffusion-limited rate forward rate constants, k_{diff} [Eq. (S26)]. The theoretical upper bound in the absence of particle-particle interactions, $k_F^{\text{upper,RP}}$ in Eq. (S27) (magenta dashed line), and k_F^{FD} in Eq. (S29) (green dotted line) are also shown, which were typically larger than the NMR-determined k_Fs.

oretical work[3,4] demonstrated that due to "competition" from neighboring scatterers (or emulsion droplets in this case), k_{diff} could increase with increasing ϕ_{Organic}. Using a variational principle, Reck and Prager[3] found an upper bound for k_F as a function of ϕ_{Organic}:

$$k_F^{\text{upper,RP}}(\phi_{\text{Organic}}) = k_{\text{diff}} \frac{\phi_{\text{Organic}}}{e^{-\phi_{\text{Organic}}} - (\phi_{\text{Organic}})^{\frac{1}{3}}\,\Gamma\left(\frac{2}{3}, \phi_{\text{Organic}}\right)} \tag{S27}$$

where $\Gamma(s, \phi)$ is the upper incomplete gamma function given by:

$$\Gamma(s, \phi) = \int_{\phi}^{\infty} x^{s-1} e^{-x} \mathrm{d}x \tag{S28}$$

A perturbative theory[4] for $k_F(\phi_{\text{Organic}})$ was also . by Felderhof and Deutch whereby:

$$k_F^{\text{FD}}(\phi_{\text{Organic}}) \approx k_{\text{diff}} \left(1 + (3\phi_{\text{Organic}})^{\frac{1}{3}} + 12.71\phi_{\text{Organic}} + \frac{3\phi_{\text{Organic}}}{2} \ln\left(\phi_{\text{Organic}}\right)\right) \quad \text{(S29)}$$

In Fig. S11, the NMR-determined k_F from both models are plotted along with the corresponding theoretical k_F^{FD} and $k_F^{\text{upper,RP}}$, which were typically larger than the NMR-determined values. Even though the models presented in Sections II A and II B were not consistent with the experiments in Fig. 7 of the main text since they do not predict an $[\text{Iso}]_{\text{tot}}$-dependence to $\delta_{\text{obs}}^{\alpha/\beta}$, the values of k_F and k_B from these models were still the same order of magnitude as k_F and k_B given in Fig. 4 of the main text, $10^{11}\text{M}^{-1}\text{s}^{-1}$ and $10^3 - 10^4\text{s}^{-1}$, respectively.

III. ACKNOWLEDGMENTS

Acknowledgements Research reported in this manuscript was supported by funding from the National Institute of Diabetes and Digestive and Kidney Diseases of the National Institutes of Health under award number R01DK116875, the Diabetes Research Institute Foundation, the National Science Foundation under CHE-1626015 and CHE-1807724, and the University of Miami Center for Computational Science. The content is solely the responsibility of the authors and does not necessarily represent the official views of the National Institutes of Health.

---

* cfraker@med.miami.edu

† jwalls@miami.edu

[1] Igumenova, T. I., Brath, U., Akke, M. & Palmer, A. G. Characterization of chemical exchange using residual dipolar coupling. *J. Am. Chem. Soc.* **129**, 13396–13397 (2007).

[2] von Smoluchowski, M. Versucheiner mathematischen theorie der koagulations kinetic kolloider lousungen. *Z. Phys. Chem.* **92**, 129–168 (1917).

[3] Reck, R. A. & Prager, S. Diffusion-controlled quenching at higher quencher concentrations. *J. Chem. Phys.* **42**, 3027–3032 (1965).

[4] Felderhof, B. U. & Deutch, J. M. Concentration dependence of the rate of diffusion-controlled reactions. *J. Chem. Phys.* **64**, 4551–4558 (1976).